CHAOS
Theory and Applications
in Applied Sciences and Engineering

e-ISSN: 2687-4539
RESEARCH ARTICLE
Vol.8 / No.1 / 2026 / pp.36-55
https://doi.org/10.51537/chaos.1740622

Stability and Bifurcation Analysis of Mpox Transmission Model

Benjamin Idoko Omede [*,1], **Sayooj Aby Jose** [α,2], **Anuwat Jirawattanapanit** [α,3] **and Olfa Boubaker** [§,4]

[*]Department of Mathematical Sciences, Prince Abubakar Audu (Formerly Kogi State) University, Anyigba, Nigeria, [α]Department of Mathematics, Faculty of Education, Phuket Rajabhat University, Thailand, [§]University of Carthage, National Institute of Applied Sciences and Technology, Tunisia.

ABSTRACT In this study, we conducted a thorough and in-depth investigation into the existence and stability of the boundary equilibria of a deterministic mathematical model for Mpox transmission to gain a deeper understanding of the disease dynamics. The investigation begins with the identification and analysis of the Mpox boundary equilibria, which include the rodent-only boundary equilibrium, the human-only boundary equilibrium, and the coexistence of the rodent and human boundary equilibria. Using center manifold analysis, it was demonstrated that both the rodent equilibrium and the human equilibrium exhibit backward bifurcation when the basic reproduction number of the Mpox transmission model is less than unity. This backward bifurcation phenomenon complicates the control and eradication of Mpox in both rodent and human populations, even when the basic reproduction number is below one. To evaluate the robustness of the model results, uncertainty and sensitivity analyses were performed using Latin Hypercube Sampling and Partial Rank Correlation Coefficient methods. The results indicate that the basic reproduction number is most sensitive to the human-to-human and rodent-to-rodent transmission rates, as well as the proportion of quarantined humans who progress to active infection, while increases in the treatment rate of infected humans and the rodent death rate significantly reduce the transmission potential of Mpox. Additionally, to underscore the importance of community education, public awareness, and enlightenment campaigns in curbing the spread of Mpox, we introduced two time-dependent control measures to the Mpox model, namely, precautionary actions taken by susceptible individuals to hinder the spread of Mpox (these actions include regular handwashing, wearing gloves when handling rodents, and avoiding direct contact with the open sores of infected humans), and the use of disinfectants (for washing clothes and cleaning of surfaces) and proper sanitation practices to increase the decay rate of the Mpox virus in the environment. Our numerical simulations indicate that each control measure is effective in reducing the spread of Mpox. However, the combined implementation of both control measures proves to be particularly effective in significantly reducing the prevalence of the disease.

KEYWORDS
Mpox
Stability
Bifurcation
Optimal control
Simulation

INTRODUCTION

Mpox, previously referred to as monkeypox (World Health Organization *et al.* 2022), is a zoonotic infection resulting from the monkeypox virus (MPXV), a double-stranded DNA virus classified within the Orthopoxvirus genus of the Poxviridae family. This viral family also includes the variola virus, responsible for smallpox, and the vaccinia virus, associated with cowpox (Branda *et al.* 2024). Mpox, an orthopoxvirus, is endemic to Central and West Africa. It was initially identified in captive monkeys in 1958 and subsequently detected in humans in 1970 in the Democratic Republic of the Congo (DRC), during the concluding phase of the global smallpox eradication campaign (Branda *et al.* 2024; Subissi *et al.* 2024). Since that time, sporadic outbreaks have occurred in various countries within West and Central Africa, predominantly impacting children residing in rural, rainforest areas. MPXV is classified into two genetically distinct clades: Clade I, formerly known as the Central African or Congo Basin clade, and Clade II, previously referred to as the West African clade. Clade II is further divided into two subclades, IIa and IIb. Clade I has been linked to more severe clinical outcomes, increased human-to-human transmissibility, and a higher case fatality rate compared to Clade II (Branda *et al.* 2024). MPXV is broadly distributed among various small rodents and primates in Africa, including dormice, squirrels, Gambian pouched rats, non-human primates, and other species. Nonetheless, the specific natural reservoirs of the virus and the mechanisms underlying its persistence in wild populations remain uncertain (Branda *et al.* 2024). Global attention was drawn to the MPXV outbreak in 2003, when the virus was reported outside of Africa for the first time, including in the United States (Reed *et al.* 2004; Larkin 2003; Stephenson 2003). Following the World Health Organization's (WHO) declaration of the outbreak as a 'Public Health Emergency of International Concern' on July 23, 2022, a total of 91,123 confirmed cases and 663 probable cases were recorded by September 30, 2023, along with 157 reported deaths across 115 countries and territories. More recently, the resurgence and rapid increase in reported MPXV cases have raised significant public health concerns (Sun *et al.* 2024).

MPXV is a zoonotic virus capable of transmission from animals to humans, as well as between individuals. Infection typically occurs through breaches in the skin or via mucous membranes during activities such as physical contact, kissing, or sexual interactions. The virus may also be transmitted through contact with contaminated materials, including clothing, bedding, or needles,

Manuscript received: 11 July 2025,
Revised: 9 February 2026,
Accepted: 13 March 2026.

[1]benjaminomede197@gmail.com
[2]sayooaby999@gmail.com (**Corresponding author**)
[3]anuwat.j@pkru.ac.th
[4]olfa.boubaker@insat.ucar.tn

as well as through prolonged inhalation of respiratory droplets. Additionally, exposure to lesion exudates, blood, or other bodily fluids from infected humans or animals can facilitate transmission. Handling infected animals, processing contaminated meat, or sustaining bites or scratches from infected animals are also recognized routes of transmission (Sun *et al.* 2024; Kumar *et al.* 2022; Kaler *et al.* 2022). The MPXV outbreak in July 2022 was primarily associated with close physical contact, particularly sexual activity, with the majority of cases occurring among men who have sex with men (MSM) (Sun *et al.* 2024; Thornhill *et al.* 2022).

Cases of vertical transmission have also been documented, including transplacental infection, wherein the virus is transmitted from an infected pregnant individual to the fetus via the placenta (Sun *et al.* 2024; Schwartz *et al.* 2023). The incubation period for human Mpox ranges from 5 to 21 days, with a typical duration of 7 to 17 days (Banuet-Martinez *et al.* 2023; Lum *et al.* 2022). This is followed by a prodromal phase lasting approximately 1 to 4 days (Banuet-Martinez *et al.* 2023). MPXV is genetically and clinically similar to the variola virus but usually leads to milder disease compared with smallpox (Araf *et al.* 2024). Nevertheless, the clinical severity can vary considerably among individuals and is influenced by underlying health conditions and contextual factors (Islam *et al.* 2023). Individuals affected during the 2022 MPXV outbreak presented with a wide spectrum of clinical manifestations, including high fever, skin rash, fatigue, headache, lymphadenopathy (particularly inguinal), sore throat, chills, nausea, shortness of breath, dysphagia, chest pain, myalgia, and, in some cases, genital necrosis. Additional symptoms included gastrointestinal disturbances such as diarrhea and vomiting potentially leading to dehydration as well as conjunctivitis, corneal involvement resulting in ocular damage, tonsillitis, pharyngitis, encephalitis, and, in rare instances, bronchopneumonia (Islam *et al.* 2023). Previous smallpox vaccination is estimated to confer approximately 85% protection against Mpox; however, the duration and long-term efficacy of this vaccine-induced immunity remain unclear (Mitjà *et al.* 2023).

Over the past two decades, mathematical modeling has become essential in the study of infectious diseases. This approach has a long history and is increasingly utilized to understand transmission patterns, design studies and public health interventions, assess the effectiveness of interventions, and prepare for and respond to outbreaks and epidemics. Epidemiology of infectious diseases is fundamentally multidisciplinary, as the spread of infections among a community is influenced not only by the biological characteristics of the pathogen and its host, but also by factors such as the interactions between hosts (and vectors, when applicable), environmental conditions, and, for humans, their healthcare utilization and reactions to health interventions (see, for example (Boubaker 2024; Yılmaz and Aydıner 2024; Wiraya *et al.* 2024)). Mathematical frameworks are utilized to illustrate the complex interactions among these factors and to incorporate information from a range of sources, such as social sciences. Various mathematical models have been created to analyze the dynamics of Mpox (see, for example (Alharbi *et al.* 2022; Ahmad *et al.* 2024; Sweilam *et al.* 2024)). For instance, Peter *et al.* (2023) formulated and examined a deterministic mathematical model to investigate the transmission dynamics of Mpox, integrating an optimal control framework alongside a cost-effectiveness analysis. Their model incorporated four control interventions: prevention of zoonotic transmission from rodents to humans, mitigation of human-to-human transmission, isolation of infected individuals, and treatment of those isolated. The study concluded that among these interventions, preventive measures targeting the reduction of transmission from rodents to humans were the most cost-effective.

Al-Shomrani *et al.* (2023) developed and conducted a comprehensive analysis of a deterministic SEIR-based model that accounts for the prodromal phase, variable infectivity levels, and hospitalization, to investigate the transmission dynamics of Mpox. El Mansouri *et al.* (2023) developed and analyzed a discrete-time mathematical model to characterize Mpox transmission dynamics within a human population. Their model was extended to include three control interventions: increasing awareness among at-risk groups via media campaigns, civil society engagement, and educational programs; implementing quarantine measures for infected individuals either at home or in hospital settings when necessary; and encouraging vaccination among susceptible individuals. Their findings indicated that all these strategies effectively reduce Mpox transmission, with the optimal choice of intervention depending on the specific objectives outlined in the model's control framework.

Aly *et al.* (2024) introduced a novel mathematical model employing fractional-order differential equations with the Caputo-Fabrizio derivative to simulate the transmission dynamics of the Mpox virus. Qureshi *et al.* (2022) developed stochastic models to simulate and forecast Mpox incidence. Their research included a comparative evaluation of a machine learning approach—namely, the multilayer perceptron (MLP) model against a conventional time series technique utilizing the Box-Jenkins methodology, specifically the ARIMA model. The findings revealed that the machine learning model outperformed the traditional time series method in terms of predictive accuracy. Okongo *et al.* (2024) developed and thoroughly analyzed a deterministic mathematical model to study Mpox transmission dynamics within an age-structured human population. Their findings indicated that reducing contact rates between susceptible and infected individuals both among children and adults can effectively lower infection rates. They further concluded that controlling the spread of Mpox relies heavily on strategies such as early diagnosis, prompt treatment, and hospitalization of severely ill patients. Omede *et al.* (2026) developed and conducted a qualitative analysis of a deterministic mathematical model to examine the influence of environmental reservoirs and host interactions on Mpox transmission dynamics. Their model incorporates all potential transmission pathways, including direct contact, vertical transmission, environmental exposure, and zoonotic (animal-to-human) transmission. Furthermore, they validated the model by fitting it to empirical data, using weekly confirmed Mpox case reports from Nigeria.

A key limitation of the study by Omede *et al.* (2026) was the absence of an investigation into the existence and stability of the Mpox boundary (endemic) equilibria. To address this gap, the present study extends their work by performing a comprehensive analysis of the existence and stability conditions of these equilibria. Additionally, we enhance the model proposed in Omede *et al.* (2026) through the incorporation of two time-dependent control measures designed to highlight the impact of community education, public awareness, and enlightenment campaigns in mitigating the transmission of Mpox. The structure of this paper is as follows: Section 2 outlines the development of the model; Section 3 provides the analytical findings; Section 4 examines the extended Mpox model with the integration of optimal control strategies; and Section 5 offers concluding observations.

MODEL DEVELOPMENT

In the work of Omede *et al.* (2026), they designed a deterministic mathematical model for Mpox co-circulating within human and rodent populations. The total human population at time t, denoted by $N_H(t)$, is stratified into six compartments of susceptible individuals denoted by $S_H(t)$, exposed individuals denoted by $E_H(t)$, quarantined individuals denoted by $Q(t)$, infected individuals denoted by $I_H(t)$, treated individuals denoted by $T_H(t)$, and recovered individuals denoted by $R_H(t)$. Similarly, the total rodent population at time t, denoted by $N_R(t)$, is divided into three compartments: susceptible rodents denoted by $S_R(t)$, exposed rodents denoted by $E_R(t)$, and infected rodents denoted by $I_R(t)$. The dynamics of the Mpox transmission model in Omede *et al.* (2026) are governed by the system of nonlinear differential equations presented in equation (1), with the descriptions of model variables and parameters provided in Table 1, 2, and 3.

$$\begin{aligned}
\frac{dS_H}{dt} &= (1-\xi I_H)\,\pi_H - \lambda_H S_H - \omega_H S_H + (1-\alpha)\,\sigma Q,\\
\frac{dE_H}{dt} &= \lambda_H S_H - (\gamma+\psi+\omega_H)\,E_H,\\
\frac{dQ}{dt} &= \gamma E_H - (\sigma+\omega_H)\,Q,\\
\frac{dI_H}{dt} &= \psi E_H + \alpha\sigma Q + \xi\pi_H I_H + \varphi\lambda_H R_H - (\tau+\delta_H+\omega_H)\,I_H,\\
\frac{dT_H}{dt} &= \tau I_H - (\theta+\phi\delta_H+\omega_H)\,T_H,\\
\frac{dR_H}{dt} &= \theta T_H - (\varphi\lambda_H+\omega_H)\,R_H,\\
\frac{dS_R}{dt} &= \pi_R - \lambda_R S_R - \omega_R S_R,\\
\frac{dE_R}{dt} &= \lambda_R S_R - (\eta+\omega_R)\,E_R,\\
\frac{dI_R}{dt} &= \eta E_R - \omega_R I_R,\\
\frac{dM}{dt} &= r_1 I_R + r_2 I_H - \omega_e M.
\end{aligned} \tag{1}$$

Where

$$\lambda_H = \frac{\beta_H I_H + \beta_{RH} I_R}{N_H} + \frac{\beta_{eH} M}{K+M}, \text{and} \quad \lambda_R = \frac{\beta_R I_R}{N_R} + \frac{\beta_{eR} M}{K+M}.$$

With initial conditions $S_H(0) > 0$, $E_H(0) \geq 0$, $Q(0) \geq 0$, $I_H(0) \geq 0$, $T_H(0) \geq 0$, $R_H(0) \geq 0$, $S_R(0) \geq 0$, $E_R(0) \geq 0$, $I_R(0) \geq 0$, and $M(0) \geq 0$.

It can be shown in Omede *et al.* (2026) that the feasible region

$$\Omega = \Omega_H \cup \Omega_R \cup \Omega_M \subset \Re_+^6 \times \Re_+^3 \times \Re_+^1. \tag{2}$$

Where

$$\Omega_H = \left\{ (S_H, E_H, Q, I_H, T_H, R_H) \in \Re_+^6 : N_H \leq \frac{\pi_H}{\omega_H} \right\},$$

$$\Omega_R = \left\{ (S_R, E_R, I_R) \in \Re_+^3 : N_R \leq \frac{\pi_R}{\omega_R} \right\},$$

and

$$\Omega_M = \left\{ M \in \Re_+^1 : M \leq \frac{r^*}{\omega_e} \left(\frac{\pi_R}{\omega_R} + \frac{\pi_H}{\omega_H} \right) \right\}.$$

Consequently, the dynamics of the Mpox model are analyzed within the positively invariant region Ω.

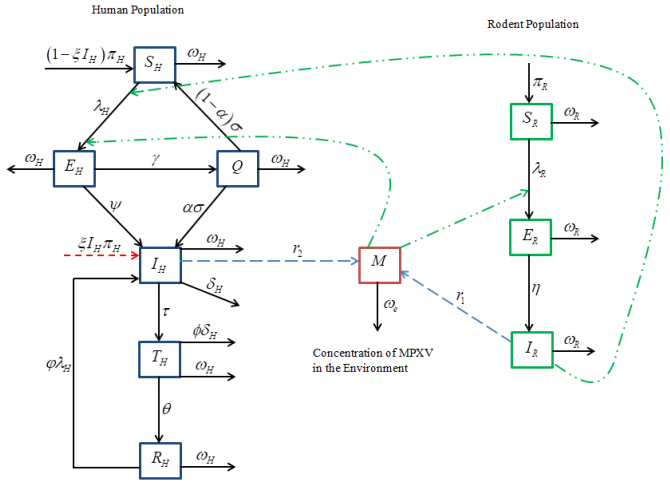

Figure 1 Schematic Diagram of the Mpox model

Human-rodent transmission is modeled through direct zoonotic contact and indirect exposure via environmental contamination, reflecting established Mpox spillover pathways. These interactions are assumed to occur at low but non-negligible rates, consistent with sporadic wildlife contact in endemic settings.

ANALYTICAL STUDY OF THE MODEL

Asymptotic Stability of the Mpox Disease-free Equilibrium

The Mpox model (1) disease-free equilibrium is given by

$$\begin{aligned}
\ell_0 &= (S_H^*, E_H^*, Q^*, I_H^*, T_H^*, R_H^*, S_R^*, E_R^*, I_R^*, M^*)\\
&= \left\{ \frac{\pi_H}{\omega_H}, 0, 0, 0, 0, 0, \frac{\pi_R}{\omega_R}, 0, 0, 0 \right\}
\end{aligned} \tag{3}$$

The basic reproduction number of the Mpox model (1) was computed in Omede *et al.* (2026) using the next generation operator method described in Van den Driessche and Watmough (2002), and it is given by

$$\begin{aligned}
\mathscr{R}_0^M = {} & \frac{\beta_H(\gamma\alpha\sigma+\psi P_3)}{P_2P_3P_4} + \frac{\xi\pi_H}{P_4} + \frac{\beta_R\eta}{P_6\omega_R}\\
& + \frac{\beta_{eH}\pi_H r_2(\gamma\alpha\sigma+\psi P_3)}{KP_2P_3P_4\omega_H\omega_e} + \frac{\beta_{eR}\pi_R\eta r_1}{KP_6\omega_R^2\omega_e} +\\
& \frac{\beta_{eR}\pi_R\eta(\gamma\alpha\sigma+\psi P_3)(\beta_{RH}r_2-\beta_H r_1)}{KP_2P_3P_4P_6\omega_R^2\omega_e} -\\
& \frac{\beta_R\eta(\gamma\alpha\sigma+\psi P_3)(\beta_{eH}\pi_H r_2+\beta_H K\omega_H\omega_e)}{KP_2P_3P_4P_6\omega_H\omega_R\omega_e}\\
& - \frac{\xi\pi_H\eta(\beta_R K\omega_R\omega_e+\beta_{eR}\pi_R r_1)}{KP_4P_6\omega_R^2\omega_e}
\end{aligned} \tag{4}$$

Where

$P_1 = (1-\alpha)\sigma$, $P_2 = \gamma+\psi+\omega_H$, $P_3 = \sigma+\omega_H$, $P_4 = \tau+\delta_H+\omega_H$, $P_5 = \theta+\phi\delta_H+\omega_H$, and $P_6 = \eta+\omega_R$. That is

$$\mathscr{R}_0^M = \mathscr{R}_0^H + \mathscr{R}_0^V + \mathscr{R}_0^R + \mathscr{R}_0^{eH} + \mathscr{R}_0^{eR} + \mathscr{R}_0^{eRH} \tag{5}$$

Where

$\mathscr{R}_0^H = \frac{\beta_H(\gamma\alpha\sigma+\psi P_3)}{P_2P_3P_4}$ represents the basic reproduction number attributable to human-to-human transmission.

$\mathscr{R}_0^V = \frac{\xi\pi_H}{P_4}$ denotes the component of the basic reproduction number resulting from vertical transmission of Mpox from mother to child.

Table 1 Interpretation of the state variables associated to the Mpox model (1)

Variable	Interpretation	Initial Value	Unit
S_H	Number of Susceptible Humans.	217000000	Person
E_H	Number of Exposed Humans to Mpox.	5000	Person
Q	Number of Quarantined Humans.	100	Person
I_H	Number of Mpox Infected Humans.	50	Person
T_H	Number of Treated Humans with Mpox.	10	Person
R_H	Number of Recovered Humans from Mpox.	0	Person
S_R	Number of Susceptible Rodents.	6000	Person
E_R	Number of Exposed Rodents to Mpox.	800	Person
I_R	Number of Infected Rodents with Mpox.	80	Person
M	Environmental Concentration of Mpox.	100	Virion

$\mathscr{R}_0^R = \frac{\beta_R \eta}{P_6 \omega_R}$ represents the portion of the basic reproduction number that arises from transmission occurring between rodents.
$\mathscr{R}_0^{eH} = \frac{\beta_{eH} \pi_H r_2 (\gamma_A \sigma + \psi P_3)}{K P_2 P_3 P_4 \omega_H \omega_e}$ represents the portion of the basic reproduction number that results from environmental transmission to humans.
$\mathscr{R}_0^{eR} = \frac{\beta_{eR} \pi_R \eta r_1}{K P_6 \omega_R^2 \omega_e}$ reflects the portion of the basic reproduction number that results from environmental transmission to rodents.
$\mathscr{R}_0^{eRH} = \frac{\beta_{eR} \pi_R \eta (\gamma_A \sigma + \psi P_3)(\beta_{RH} r_2 - \beta_H r_1)}{K P_2 P_3 P_4 P_6 \omega_R^2 \omega_e} - \frac{\beta_R \eta (\gamma_A \sigma + \psi P_3)(\beta_{eH} \pi_H r_2 + \beta_H K \omega_H \omega_e)}{K P_2 P_3 P_4 P_6 \omega_H \omega_R \omega_e} - \frac{\xi \pi_H \eta (\beta_R K \omega_R \omega_e + \beta_{eR} \pi_R r_1)}{K P_4 P_6 \omega_R^2 \omega_e}$ captures the portion of the basic reproduction number that results from indirect transmission, beginning in the environment, moving to rodents, and ultimately reaching humans.

A detailed investigation of the local stability of the disease-free equilibrium was conducted in Omede *et al.* (2026), from which the following theorem is derived.

Theorem 1. *The disease-free equilibrium (ℓ_0) of the Mpox model (1) is locally asymptotically stable if $\mathscr{R}_0^M < 1$, and unstable if $\mathscr{R}_0^M > 1$.*

Analysis of Boundary Equilibrium: Existence and Stability

In this part, we will investigate the presence and stability of the steady states of the Mpox model (1), which occur when the variables representing Mpox infections are non-zero. Therefore, by applying the method in (Omede *et al.* 2023b, 2024b), the possible steady states of the Mpox model (1) are presented as follows

1. Rodent-only boundary equilibrium,

   $\zeta_R = (0,0,0,0,0,0,S_R^{**}, E_R^{**}, I_R^{**}, M^{**})$ (in this case, Mpox is present in only the rodent population).

2. Human-only boundary equilibrium,

   $\zeta_H = (S_H^{**}, E_H^{**}, Q^{**}, I_H^{**}, T_H^{**}, R_H^{**}, 0, 0, 0, M^{**})$ (here, Mpox is present in only the human population. This is possible through travel-associated Mpox cases).

3. Coexistence of Human and Rodent boundary equilibria,

   $\zeta_{HR} = (S_H^{**}, E_H^{**}, Q^{**}, I_H^{**}, T_H^{**}, R_H^{**}, S_H^{**}, E_H^{**}, I_H^{**}, M^{**})$ (in this case, Mpox is co-circulating in the human and rodent population)

The Mpox model (1), evaluated at steady state, yields the following expressions in terms of the infection rates:

$$\begin{aligned} \lambda_H^{**} &= \frac{\beta_H I_H^{**} + \beta_{RH} I_R^{**}}{N_H^{**}} + \frac{\beta_{eH} M^{**}}{K + M^{**}}, \text{and} \\ \lambda_R^{**} &= \frac{\beta_R I_R^{**}}{N_R^{**}} + \frac{\beta_{eR} M^{**}}{K + M^{**}}. \end{aligned} \tag{6}$$

Where

$$N_H^{**} = S_H^{**} + E_H^{**} + Q^{**} + I_H^{**} + T_H^{**} + R_H^{**}, \tag{7}$$

and

$$N_R^{**} = S_R^{**} + E_R^{**} + I_R^{**}. \tag{8}$$

Table 2 Interpretation of the parameters associated to the Mpox model (1)

Parameter	Interpretation	Baseline value	Unit	Reference
π_H	Human recruitment rate.	36.61	Per 1000 persons	(Statista 2025a)
π_R	Rodent recruitment rate.	0.2		(Peter *et al.* 2022)
ξ	Proportion of individuals who were infected with Mpox at birth or migrated while carrying the Mpox infection.	1×10^{-8}	Per week	(Omede *et al.* 2026)
β_H	Transmission probability between infected humans and susceptible humans.	0.0334	Per week	(Omede *et al.* 2026)
β_{RH}	Transmission probability from infected rodents to susceptible humans.	0.0052466	Per week	(Omede *et al.* 2026)
β_R	Transmission probability from infected rodents to susceptible rodents.	0.0003	Per week	(Adepoju and Ibrahim 2024)
β_{eH}	Transmission probability from the environmental concentration of Mpox to susceptible humans.	2.4901×10^{-8}	Per week	(Omede *et al.* 2026)
β_{eR}	Transmission probability from the environmental concentration of Mpox to susceptible rodents.	1×10^{-8}	Per week	(Omede *et al.* 2026)
ω_H	Natural death rate for humans.	12.43	Per 1000 persons	(Statista 2025b)
ω_R	Death rate for rodents.	0.002	Per week	(Peter *et al.* 2022)
ω_e	Mpox virus decay rate.	0.35	Per week	(Omede *et al.* 2026)
τ	Treatment rate of infected individuals.	0.01	Per week	(Omede *et al.* 2026)
δ_H	Mpox disease-induced death rate for humans.	0.003286	Per week	(Peter *et al.* 2022)
γ	Quarantined rate of exposed individuals.	0.4	Per week	(Omede *et al.* 2026)
ψ	Progression rate from exposed class to infected class for humans.	0.016744	Per week	(Peter *et al.* 2022)
σ	Human progression rate from quarantined class to either infected or susceptible class.	0.1	Per week	(Omede *et al.* 2026)
α	Fraction of quarantined humans that progressed to the infected class.	0.3	Per week	(Omede *et al.* 2026)

Table 3 Continuation of the Interpretation of the parameters associated to the Mpox model (1)

Parameter	Interpretation	Baseline value	Unit	Reference
$1-\alpha$	Remaining fraction of quarantined humans that progressed back to being susceptible again.	0.7	Per week	(Omede *et al.* 2026)
η	Rodent progression rate from exposed to being infected with Mpox.	0.34	Per week	(Omede *et al.* 2026)
θ	Recovery rate of treated individuals.	0.83	Per week	(Elsonbaty *et al.* 2024)
ϕ	Modification parameter representing the decrease in Mpox-related mortality due to medical treatment.	0.01	Per week	(Omede *et al.* 2026)
φ	Modification parameter that accounts for re-infection after recovery from Mpox.	0.014	Per week	(Omede *et al.* 2026)
r_1	Shedding rate of Mpox in the environment from infected rodents.	0.1	Per week	(Omede *et al.* 2026)
r_2	Shedding rate of Mpox in the environment from infected humans.	0.07	Per week	(Omede *et al.* 2026)
K	Carrying capacity.	10000		(Omede *et al.* 2026)

With

$$
\begin{aligned}
S_H^{**} &= \frac{\pi_H P_2 P_3 P_5(\varphi\lambda_H^{**}+\omega_H)(P_4-\xi\pi_H)-\lambda_H^{**}\pi_H\varphi\tau\theta P_2 P_3}{(\varphi\lambda_H^{**}+\omega_H)\Delta_2-\lambda_H^{**}\varphi\tau\theta\Delta_1},\\
E_H^{**} &= \frac{\lambda_H^{**}\pi_H P_3 P_5(\varphi\lambda_H^{**}+\omega_H)(P_4-\xi\pi_H)-\lambda_H^{**2}\pi_H\varphi\tau\theta P_3}{(\varphi\lambda_H^{**}+\omega_H)\Delta_2-\lambda_H^{**}\varphi\tau\theta\Delta_1},\\
Q^{**} &= \frac{\lambda_H^{**}\pi_H\gamma P_5(\varphi\lambda_H^{**}+\omega_H)(P_4-\xi\pi_H)-\lambda_H^{**2}\pi_H\varphi\tau\theta\gamma}{(\varphi\lambda_H^{**}+\omega_H)\Delta_2-\lambda_H^{**}\varphi\tau\theta\Delta_1},\\
I_H^{**} &= \frac{\lambda_H^{**}\pi_H P_5(\varphi\lambda_H^{**}+\omega_H)(\gamma\alpha\sigma+\psi P_3)}{(\varphi\lambda_H^{**}+\omega_H)\Delta_2-\lambda_H^{**}\varphi\tau\theta\Delta_1},\\
T_H^{**} &= \frac{\lambda_H^{**}\pi_H\tau(\varphi\lambda_H^{**}+\omega_H)(\gamma\alpha\sigma+\psi P_3)}{(\varphi\lambda_H^{**}+\omega_H)\Delta_2-\lambda_H^{**}\varphi\tau\theta\Delta_1},\\
R_H^{**} &= \frac{\lambda_H^{**}\pi_H\tau\theta(\varphi\lambda_H^{**}+\omega_H)(\gamma\alpha\sigma+\psi P_3)}{(\varphi\lambda_H^{**}+\omega_H)\Delta_2-\lambda_H^{**}\varphi\tau\theta\Delta_1},\\
S_R^{**} &= \frac{\pi_R}{\lambda_R^{**}+\omega_R}, E_R^{**}=\frac{\lambda_R^{**}\pi_R}{(\lambda_R^{**}+\omega_R)P_6},\\
I_R^{**} &= \frac{\lambda_R^{**}\pi_R\eta}{(\lambda_R^{**}+\omega_R)\omega_R P_6},\\
M^{**} &= \frac{\lambda_R^{**}\pi_R\eta r_1}{(\lambda_R^{**}+\omega_R)\omega_R\omega_e P_6}+\\
&\quad\frac{\lambda_H^{**}\pi_H r_2 P_5(\varphi\lambda_H^{**}+\omega_H)(\gamma\alpha\sigma+\psi P_3)}{(\varphi\lambda_H^{**}+\omega_H)\omega_e\Delta_2-\lambda_H^{**}\varphi\tau\theta\omega_e\Delta_1},
\end{aligned}
\tag{9}
$$

Where

$P_1=(1-\alpha)\sigma$, $P_2=\gamma+\psi+\omega_H$, $P_3=\sigma+\omega_H$, $P_4=\tau+\delta_H+\omega_H$, $P_5=\theta+\phi\delta_H+\omega_H$, $P_6=\eta+\omega_R$, $\Delta_1=(\lambda_H^{**}+\omega_H)P_2P_3-\lambda_H^{**}\gamma P_1$, and $\Delta_2=P_5\left(\Delta_1(P_4-\xi\pi_H)+\lambda_H^{**}\xi\pi_H(\gamma\alpha\sigma+\psi P_3)\right)$. The equilibria of the Mpox model (1) can be found by inputting the steady-state components into the equations in (6) and solving for the fixed points of the system as outlined below

$$
g(\chi)=\begin{pmatrix} g_1\left(\lambda_H^{**},\lambda_R^{**}\right)\\ g_2\left(\lambda_H^{**},\lambda_R^{**}\right)\end{pmatrix}, where \quad \chi=\begin{pmatrix}\lambda_H^{**}\\ \lambda_R^{**}\end{pmatrix}, \tag{10}
$$

both g_1 and g_2 correspond to the right-hand sides of the equations for λ_H^{**} and λ_R^{**} in (6), respectively.

Rodent-only Boundary Equilibrium: This equilibrium characterizes an ecological scenario where Mpox remains endemic in the rodent population without spillover to humans. Such a situation reflects the recognized role of rodents as natural reservoirs of MPXV, where sustained transmission can occur independently of humans. In this state, environmental contamination may remain non-zero due to continuous viral shedding by infected rodents. This equilibrium therefore captures the enzootic maintenance of Mpox in wildlife, which serves as a persistent source of potential spillover to humans.

Thus, the rodent-only boundary equilibrium denoted by ζ_R, is given by

$$\zeta_R = (0,0,0,0,0,0,S_R^{**},E_R^{**},I_R^{**},M^{**}), \tag{11}$$

with

$$\begin{aligned} S_R^{**} &= \frac{\pi_R}{\lambda_R^{**}+\omega_R}, E_R^{**} = \frac{\lambda_R^{**}\pi_R}{(\lambda_R^{**}+\omega_R)P_6}, I_R^{**} = \frac{\lambda_R^{**}\pi_R\eta}{(\lambda_R^{**}+\omega_R)\omega_R P_6}, \\ M^{**} &= \frac{\lambda_R^{**}\pi_R\eta r_1}{(\lambda_R^{**}+\omega_R)\omega_R\omega_e P_6}, \end{aligned} \tag{12}$$

By solving the fixed-point equation $g_2\left(0,\lambda_R^{**}\right) = \lambda_R^{**}$, one may ascertain whether the rodent-only boundary equilibrium exists. Solving this fixed-point equation λ_R^{**} leads to the following polynomial:

$$\mathscr{L}(\lambda_R^{**}) = \lambda_R^{**}\left(\Phi_1\lambda_R^{**2} + \Phi_2\lambda_R^{**} + \Phi_3\right) = 0 \tag{13}$$

Where

$$\begin{aligned} \Phi_1 &= \pi_R P_6\left(K\omega_R\omega_e P_6 + \pi_R\eta r_1\right), \\ \Phi_2 &= \pi_R\omega_R P_6\left(\left(K\omega_R\omega_e P_6 + \pi_R\eta r_1\right) + K\omega_R\omega_e P_6\right) - \\ &\quad \beta_R\pi_R\eta\left(K\omega_R\omega_e P_6 + \pi_R\eta r_1\right) - \beta_{eR}\pi_R^2\eta r_1 P_6, \\ \Phi_3 &= \pi_R K\omega_R^3\omega_e P_6^2\left(1-\left(\mathscr{R}_0^R + \mathscr{R}_0^{eR}\right)\right). \end{aligned} \tag{14}$$

We can express Φ_3 as

$$\Phi_3 = \pi_R K\omega_R^3\omega_e P_6^2\left(1-\mathscr{R}_0^{MR*}\right),$$

with

$$\mathscr{R}_0^{MR*} = \mathscr{R}_0^R + \mathscr{R}_0^{eR}.$$

The solution to $\mathscr{L}\left(\lambda_R^{**}\right)$ in (13) are $\lambda_R^{**} = 0$ and $\Phi_1\lambda_R^{**2} + \Phi_2\lambda_R^{**} + \Phi_3 = 0$. Specifically, $\lambda_R^{**} = 0$ stands for the Mpox disease-free equilibrium point, and its stability has already been investigated. In contrast, $\Phi_1\lambda_R^{**2} + \Phi_2\lambda_R^{**} + \Phi_3 = 0$ denotes the rodent-only boundary (endemic) equilibrium. The polynomial $\mathscr{L}\left(\lambda_R^{**}\right)$ in (13) suggests the presence of backward bifurcation, which is frequently observed when a stable endemic equilibrium and a stable disease-free equilibrium point coexist, provided that the basic reproduction number is below one (see, for instance (Gumel 2012; Omame *et al.* 2022; Omede *et al.* 2024a; Jose *et al.* 2023b; Omame *et al.* 2021; Jose *et al.* 2023a)). The Mpox model's backward bifurcation feature makes it biologically challenging to effectively control Mpox infection in rodent populations when the basic reproduction number is less than one. Backward bifurcation necessitates the existence of multiple boundary (endemic) equilibria. Hence, we need to consider three cases for the equation $\Phi_1\lambda_R^{**2} + \Phi_2\lambda_R^{**} + \Phi_3 = 0$, determined by the sign combinations of Φ_2 and Φ_3, while noting that Φ_1 remains strictly positive. The cases are;

1. When $\Phi_2 < 0$ and $\Phi_3 = 0$ or $\Phi_2^2 - 4\Phi_1\Phi_3 = 0$, the equation $\mathscr{L}\left(\lambda_R^{**}\right)$ has exactly one positive root, and a backward bifurcation cannot occur.

2. When $\Phi_2 < 0$, $\Phi_3 > 0$ and $\Phi_2^2 - 4\Phi_1\Phi_3 > 0$, the equation $\mathscr{L}\left(\lambda_R^{**}\right)$ yields two boundary equilibria (i.e., two positive solutions), indicating the potential for a backward bifurcation.

3. Otherwise, none exists.

Nonetheless, it is important to be aware that $\Phi_3 > 0$ if $\mathscr{R}_0^{MR*} < 1$, and $\Phi_3 < 0$ if $\mathscr{R}_0^{MR*} > 1$. As a result, the following theorem follows from the investigation above.

Theorem 2. *The rodent-only boundary equilibrium of the Mpox model (1) has;*

1. *Exactly one distinct boundary equilibrium if* $\Phi_3 < 0$ *(i.e.* $\mathscr{R}_0^{MR*} > 1$*)*

2. *Exactly one distinct boundary equilibrium if* $\Phi_2 < 0$*, and* $\Phi_3 = 0$ *or* $\Phi_2^2 - 4\Phi_1\Phi_3 = 0$.

3. *Exactly two boundary equilibria if* $\Phi_3 > 0$ *(i.e.* $\mathscr{R}_0^{MR*} < 1$*),* $\Phi_2 < 0$ *and* $\Phi_2^2 - 4\Phi_1\Phi_3 > 0$.

4. *Otherwise, there would be no boundary equilibrium.*

Multiple boundary equilibria exist, indicating a backward bifurcation, if and only if $\mathscr{R}_0^{MR*} < 1$, as seen in case 3 of the rodent-only of the Mpox model (1).

Human-only Boundary Equilibrium: The human-only boundary equilibrium corresponds to a transmission regime in which Mpox circulates within the human population while rodent infection is absent. This situation is consistent with outbreak settings dominated by human-to-human transmission, such as close-contact networks or healthcare associated spread, where zoonotic spillover is limited during the outbreak period. Environmental viral contamination may still play a role through indirect transmission mechanisms. This equilibrium allows assessment of Mpox persistence driven primarily by human behavioral and contact patterns.

Thus, the human-only boundary equilibrium represented by ζ_H, is expressed as

$$\zeta_H = (S_H^{**},E_H^{**},Q^{**},I_H^{**},T_H^{**},R_H^{**},0,0,0,M^{**}), \tag{15}$$

with

$$\begin{aligned} S_H^{**} &= \frac{\pi_H P_2P_3P_5(\varphi\lambda_H^{**}+\omega_H)(P_4-\xi\pi_H) - \lambda_H^{**}\pi_H\varphi\tau\theta P_2P_3}{(\varphi\lambda_H^{**}+\omega_H)\Delta_2 - \lambda_H^{**}\varphi\tau\theta\Delta_1}, \\ E_H^{**} &= \frac{\lambda_H^{**}\pi_H P_3P_5(\varphi\lambda_H^{**}+\omega_H)(P_4-\xi\pi_H) - \lambda_H^{**2}\pi_H\varphi\tau\theta P_3}{(\varphi\lambda_H^{**}+\omega_H)\Delta_2 - \lambda_H^{**}\varphi\tau\theta\Delta_1}, \\ Q^{**} &= \frac{\lambda_H^{**}\pi_H\gamma P_5(\varphi\lambda_H^{**}+\omega_H)(P_4-\xi\pi_H) - \lambda_H^{**2}\pi_H\varphi\tau\theta\gamma}{(\varphi\lambda_H^{**}+\omega_H)\Delta_2 - \lambda_H^{**}\varphi\tau\theta\Delta_1}, \\ I_H^{**} &= \frac{\lambda_H^{**}\pi_H P_5(\varphi\lambda_H^{**}+\omega_H)(\gamma\alpha\sigma+\psi P_3)}{(\varphi\lambda_H^{**}+\omega_H)\Delta_2 - \lambda_H^{**}\varphi\tau\theta\Delta_1}, \\ T_H^{**} &= \frac{\lambda_H^{**}\pi_H\tau(\varphi\lambda_H^{**}+\omega_H)(\gamma\alpha\sigma+\psi P_3)}{(\varphi\lambda_H^{**}+\omega_H)\Delta_2 - \lambda_H^{**}\varphi\tau\theta\Delta_1}, \\ R_H^{**} &= \frac{\lambda_H^{**}\pi_H\tau\theta(\varphi\lambda_H^{**}+\omega_H)(\gamma\alpha\sigma+\psi P_3)}{(\varphi\lambda_H^{**}+\omega_H)\Delta_2 - \lambda_H^{**}\varphi\tau\theta\Delta_1}, \\ M^{**} &= \frac{\lambda_H^{**}\pi_H r_2P_5(\varphi\lambda_H^{**}+\omega_H)(\gamma\alpha\sigma+\psi P_3)}{(\varphi\lambda_H^{**}+\omega_H)\omega_e\Delta_2 - \lambda_H^{**}\varphi\tau\theta\omega_e\Delta_1}, \end{aligned} \tag{16}$$

Where

$P_1 = (1-\alpha)\sigma$, $P_2 = \gamma+\psi+\omega_H$, $P_3 = \sigma+\omega_H$, $P_4 = \tau+\delta_H+\omega_H$, $P_5 = \theta+\phi\delta_H+\omega_H$, $P_6 = \eta+\omega_R$, $\Delta_1 = (\lambda_H^{**}+\omega_H)P_2P_3 - \lambda_H^{**}\gamma P_1$, and $\Delta_2 = P_5\left(\Delta_1(P_4-\xi\pi_H) + \lambda_H^{**}\xi\pi_H(\gamma\alpha\sigma+\psi P_3)\right)$.
The presence of a boundary equilibrium corresponding exclusively to the human population is established through analysis of the fixed-point condition $g_1\left(\lambda_H^{**},0\right) = \lambda_H^{**}$. Solving this fixed-point equation for the unknown λ_H^{**} leads to the formulation of an associated polynomial equation

$$\mathscr{T}\left(\lambda_H^{**}\right) = \nabla_1\lambda_H^{**4} + \nabla_2\lambda_H^{**3} + \nabla_3\lambda_H^{**2} + \nabla_4\lambda_H^{**} + \nabla_5 \tag{17}$$

where

$$\begin{aligned}
\nabla_1 &= D_3D_6,\\
\nabla_2 &= D_3D_7 + D_4D_6 - D_1\left(\beta_H + \beta_{eH}r_2D_3\right),\\
\nabla_3 &= D_3D_8 + D_4D_7 + D_5D_6 - D_1\left(\beta_H D_7 + \beta_{eH}r_2D_4\right) -\\
&\quad D_2\left(\beta_H D_6 + \beta_{eH}r_2D_3\right),\\
\nabla_4 &= D_4D_8 + D_5D_7 - \beta_H\left(D_1D_8 + D_2D_7\right) -\\
&\quad \beta_{eH}r_2\left(D_1D_5 + D_2D_4\right),\\
\nabla_5 &= \pi_H\omega_H^3\omega_e P_2^2P_3^2P_4P_5^2K\left(1 - \mathscr{R}_0^{MH*}\right)
\end{aligned} \tag{18}$$

with

$$\begin{aligned}
&\mathscr{R}_0^{MH*} = \mathscr{R}_0^H + \mathscr{R}_0^V + \mathscr{R}_0^{eH}, D_1 = \pi_H\varphi P_5(\gamma\alpha\sigma + \psi P_3),\\
&D_2 = \pi_H\omega_H P_5(\gamma\alpha\sigma + \psi P_3),\\
&D_3 = \pi_H\varphi(P_5(P_4 - \xi\pi_H) - \tau\theta)(\gamma + P_3) +\\
&\pi_H\varphi(\gamma\alpha\sigma + \psi P_3)(P_5 + \tau\theta + \tau),\\
&D_4 = \pi_H\omega_H\left((\gamma\alpha\sigma + \psi P_3)(\tau\theta + \tau + P_5) + P_5(P_4 - \xi\pi_H)(\gamma + P_3)\right)\\
&+ \pi_H\varphi P_2P_3(P_5(P_4 - \xi\pi_H) - \tau\theta),\\
&D_5 = \pi_H\omega_H P_2P_3P_5(P_4 - \xi\pi_H),\\
&D_6 = \pi_H\varphi r_2P_5(\gamma\alpha\sigma + \psi P_3) + K\omega_e Z_1,\\
&D_7 = \pi_H\omega_H r_2P_5(\gamma\alpha\sigma + \psi P_3) + K\omega_e Z_2,\\
&D_8 = K\omega_e Z_3,\\
&Z_1 = \varphi P_5((P_2P_3 - \gamma P_1)(P_4 - \xi\pi_H) + \xi\pi_H(\gamma\alpha\sigma + \psi P_3)) -\\
&\varphi\tau\theta(P_2P_3 - \gamma P_1),\\
&Z_2 = \omega_H P_5((P_2P_3 - \gamma P_1)(P_4 - \xi\pi_H) + \xi\pi_H(\gamma\alpha\sigma + \psi P_3)) +\\
&\omega_H\varphi P_2P_3(P_5(P_4 - \xi\pi_H) - \tau\theta),\\
&Z_3 = \omega_H^2P_2P_3P_5(P_4 - \xi\pi_H)
\end{aligned} \tag{19}$$

As seen from equation (17), ∇_1 is strictly positive due to the non-negativity of all model parameters. In addition, ∇_5 remains positive provided that $\mathscr{R}_0^{MH} < 1$. Under these conditions, the admissible positive roots of (17) are governed by the sign configuration of the coefficients ∇_2, ∇_3, and ∇_4. The root structure is examined by invoking Descartes' sign criterion on the polynomial $\mathscr{T}(x) = \nabla_1x^4 + \nabla_2x^3 + \nabla_3x^2 + \nabla_4x + \nabla_5$, with $x = \lambda_H^{**}$, leading to the results stated below.

Theorem 3. *The human-only boundary equilibrium of the Mpox model (1)*

1. *Has only one boundary equilibrium if $\mathscr{R}_0^{MH*} > 1$ and any of the following conditions are met*
   - *(i)* $\nabla_2 > 0, \nabla_3 > 0, \nabla_4 > 0$;
   - *(ii)* $\nabla_2 < 0, \nabla_3 < 0, \nabla_4 < 0$;
   - *(iii)* $\nabla_2 > 0, \nabla_3 < 0, \nabla_4 < 0$;
   - *(iv)* $\nabla_2 > 0, \nabla_3 > 0, \nabla_4 < 0$;
2. *Could have 2 or more boundary equilibria if $\mathscr{R}_0^{HM*} > 1$ and any of the following conditions hold*
   - *(i)* $\nabla_2 < 0, \nabla_3 > 0, \nabla_4 < 0$;
   - *(ii)* $\nabla_2 < 0, \nabla_3 < 0, \nabla_4 > 0$;
   - *(iii)* $\nabla_2 > 0, \nabla_3 < 0, \nabla_4 > 0$;
   - *(iv)* $\nabla_2 < 0, \nabla_3 > 0, \nabla_4 > 0$;
3. *Could have 2 or more boundary equilibria if $\mathscr{R}_0^{MH*} < 1$ and any, or all, ∇_2, ∇_3, and ∇_4 are less than zero.*

As established in the third statement of Theorem 3, the coexistence of more than one boundary equilibrium when $\mathscr{R}_0^{MH} < 1$ reveals the possibility of complex dynamical behavior, suggesting that stability transitions may occur below the classical threshold value.

Coexistence of Human and Rodent Boundary Equilibria: This equilibrium describes a coupled endemic state in which Mpox persists simultaneously in both human and rodent populations, with the environment acting as a shared viral reservoir. Biologically, this scenario reflects repeated spillover and feedback between wildlife reservoir and human hosts, a hallmark of Mpox ecology in endemic regions. The presence of environmental MPXV further reinforces persistence by sustaining indirect transmission pathways. This equilibrium captures the full ecological complexity of Mpox transmission across multiple hosts.

Here, the coexistence of human and rodent boundary equilibria represented by ζ_{HR}, is expressed as

$$\zeta_{HR} = (S_H^{**}, E_H^{**}, Q^{**}, I_H^{**}, T_H^{**}, R_H^{**}, S_H^{**}, E_H^{**}, I_H^{**}, M^{**}), \tag{20}$$

Substituting (7) and (9) into the expression λ_H^{**} in (6), we obtained polynomial

$$\begin{aligned}
\mathcal{W}_H\left(\lambda_H^{**}, \lambda_R^{**}\right) = {}& \Theta_1\lambda_H^{**5}\lambda_R^{**2} + \Theta_2\lambda_H^{**5}\lambda_R^{**} + \Theta_3\lambda_H^{**5} +\\
&\Theta_4\lambda_H^{**4}\lambda_R^{**2} + \Theta_5\lambda_H^{**4}\lambda_R^{**} + \Theta_6\lambda_H^{**4} +\\
&\Theta_7\lambda_H^{**3}\lambda_R^{**2} + \Theta_8\lambda_H^{**3}\lambda_R^{**} + \Theta_9\lambda_H^{**3} +\\
&\Theta_{10}\lambda_H^{**2}\lambda_R^{**2} + \Theta_{11}\lambda_H^{**2}\lambda_R^{**} + \Theta_{12}\lambda_H^{**2} +\\
&\Theta_{13}\lambda_H^{**}\lambda_R^{**2} + \Theta_{14}\lambda_H^{**}\lambda_R^{**} + \Theta_{15}\lambda_H^{**} -\\
&\Theta_{16}\lambda_R^{**2} - \Theta_{17}\lambda_R^{**} = 0.
\end{aligned} \tag{21}$$

Where

$$\begin{aligned}
\Theta_1 &= a_6y_6,\\
\Theta_2 &= a_7y_6 + a_6y_7,\\
\Theta_3 &= a_7y_7,\\
\Theta_4 &= a_8y_6 + a_6y_8 - a_6y_1 - \beta_{eH}a_1y_6,\\
\Theta_5 &= a_9y_6 + a_8y_7 + a_7y_8 + a_6y_9 - a_7y_1 - a_6y_2 - \beta_{eH}a_1y_7 -\\
&\quad \beta_{eH}a_2y_6,\\
\Theta_6 &= a_9y_7 + a_7y_9 - a_7y_2 - \beta_{eH}a_2y_7,\\
\Theta_7 &= a_{10}y_6 + a_8y_8 + a_6y_{10} - a_8y_1 - a_6y_3 - \beta_{eH}a_1y_8 - \beta_{eH}a_3y_6,\\
\Theta_8 &= a_{11}y_6 + a_{10}y_7 + a_9y_8 + a_8y_9 + a_7y_{10} + a_6y_{11} - a_9y_1 - a_8y_2\\
&\quad - a_7y_3 - a_6y_4 - \beta_{eH}a_1y_9 - \beta_{eH}a_2y_8 - \beta_{eH}a_3y_7 - \beta_{eH}a_4y_6,\\
\Theta_9 &= a_{11}y_7 + a_9y_9 + a_7y_{11} - a_9y_2 - a_7y_4 - \beta_{eH}a_2y_9 - \beta_{eH}a_4y_7,\\
\Theta_{10} &= a_{10}y_8 + a_8y_{10} - a_{10}y_1 - a_8y_3 - a_6y_5 - \beta_{eH}a_1y_{10} -\\
&\quad \beta_{eH}a_3y_8 - \beta_{eH}a_5y_6,\\
\Theta_{11} &= a_{11}y_8 + a_{10}y_9 + a_9y_{10} + a_8y_{11} - a_{11}y_1 - a_{10}y_2 - a_9y_3 -\\
&\quad a_8y_4 - a_7y_5 - \beta_{eH}a_1y_{11} - \beta_{eH}a_2y_{10} - \beta_{eH}a_3y_9 - \beta_{eH}a_4y_8\\
&\quad - \beta_{eH}a_5a_7,\\
\Theta_{12} &= a_{11}y_9 + a_9y_{11} - a_{11}y_2 - a_9y_4 - \beta_{eH}a_2y_{11} - \beta_{eH}a_4y_9,\\
\Theta_{13} &= a_{10}y_{10} - a_{10}y_3 - a_8y_5 - \beta_{eH}a_3y_{10} - \beta_{eH}a_5y_8,\\
\Theta_{14} &= a_{11}y_{10} + a_{10}y_{11} - a_{11}y_3 - a_{10}y_4 - a_9y_5 - \beta_{eH}a_3y_{11} -\\
&\quad \beta_{eH}a_4y_{10} - \beta_{eH}a_5y_9,\\
\Theta_{15} &= \frac{a_{11}y_{11}P_4}{(P_4 - \xi\pi_H)}\left(1 - \left(\mathscr{R}_0^H + \mathscr{R}_0^V + \omega_e\mathscr{R}_0^{eH}\right)\right),\\
\Theta_{16} &= a_{10}y_5 + \beta_{eH}a_5y_{10},\\
\Theta_{17} &= a_{11}y_5 + \beta_{eH}a_5y_{11}.
\end{aligned}$$

With

$$
\begin{aligned}
a_1 &= \pi_R \eta r_1 Z_1 + \omega_R \omega_e P_6 Z_4,\\
a_2 &= \omega_R^2 \omega_e P_6 Z_4,\\
a_3 &= \pi_R \eta r_1 Z_2 + \omega_R \omega_e P_6 Z_5,\\
a_4 &= \omega_R^2 \omega_e P_6 Z_5,\\
a_5 &= \pi_R \eta r_1 Z_3,\\
a_6 &= K\omega_R \omega_e P_6 Z_1 + \pi_R \eta r_1 Z_1 + \omega_R \omega_e P_6 Z_4,\\
a_7 &= K\omega_R^2 \omega_e P_6 Z_1 + \omega_R^2 \omega_e P_6 Z_4,\\
a_8 &= K\omega_R \omega_e P_6 Z_2 + \pi_R \eta r_1 Z_2 + \omega_R \omega_e P_6 Z_5,\\
a_9 &= K\omega_R^2 \omega_e P_6 Z_2 + \omega_R^2 \omega_e P_6 Z_5,\\
a_{10} &= K\omega_R \omega_e P_6 Z_3 + \pi_R \eta r_1 Z_3,\\
a_{11} &= K\omega_R^2 \omega_e P_6 Z_3,\\
y_1 &= \beta_H \pi_H \varphi \omega_R P_5 P_6 \left(\gamma\alpha\sigma + \psi P_3\right) + \beta_{RH} \pi_R \eta Z_1,\\
y_2 &= \beta_H \pi_H \varphi \omega_R^2 P_5 P_6 \left(\gamma\alpha\sigma + \psi P_3\right),\\
y_3 &= \beta_H \pi_H \omega_H \omega_R P_5 P_6 \left(\gamma\alpha\sigma + \psi P_3\right) + \beta_{RH} \pi_R \eta Z_2,\\
y_4 &= \beta_H \pi_H \omega_H \omega_R^2 P_5 P_6 \left(\gamma\alpha\sigma + \psi P_3\right),\\
y_5 &= \beta_{RH} \pi_R \eta Z_3,\\
y_6 &= \omega_R P_6 D_3,\\
y_7 &= \omega_R^2 P_6 D_3,\\
y_8 &= \omega_R P_6 D_4,\\
y_9 &= \omega_R^2 P_6 D_4,\\
y_{10} &= \omega_R P_6 D_5,\\
y_{11} &= \omega_R^2 P_6 D_5.
\end{aligned}
$$

And

$$
\begin{aligned}
D_1 &= \pi_H \varphi P_5(\gamma\alpha\sigma + \psi P_3),\\
D_2 &= \pi_H \omega_H P_5(\gamma\alpha\sigma + \psi P_3),\\
D_3 &= \pi_H \varphi(P_5(P_4 - \xi\pi_H) - \tau\theta)(\gamma + P_3) +\\
&\quad \pi_H \varphi(\gamma\alpha\sigma + \psi P_3)(P_5 + \tau\theta + \tau),\\
D_4 &= \pi_H \omega_H \left((\gamma\alpha\sigma + \psi P_3)(\tau\theta + \tau + P_5) + P_5(P_4 - \xi\pi_H)(\gamma + P_3)\right)\\
&\quad + \pi_H \varphi P_2 P_3 (P_5(P_4 - \xi\pi_H) - \tau\theta),\\
D_5 &= \pi_H \omega_H P_2 P_3 P_5 (P_4 - \xi\pi_H),\\
D_6 &= \pi_H \varphi r_2 P_5(\gamma\alpha\sigma + \psi P_3) + K\omega_e Z_1,\\
D_7 &= \pi_H \omega_H r_2 P_5(\gamma\alpha\sigma + \psi P_3) + K\omega_e Z_2,\\
D_8 &= K\omega_e Z_3,\\
Z_1 &= \varphi P_5((P_2 P_3 - \gamma P_1)(P_4 - \xi\pi_H) + \xi\pi_H(\gamma\alpha\sigma + \psi P_3))\\
&\quad - \varphi\tau\theta(P_2 P_3 - \gamma P_1),\\
Z_2 &= \omega_H P_5((P_2 P_3 - \gamma P_1)(P_4 - \xi\pi_H) + \xi\pi_H(\gamma\alpha\sigma + \psi P_3))\\
&\quad + \omega_H \varphi P_2 P_3 (P_5(P_4 - \xi\pi_H) - \tau\theta),\\
Z_3 &= \omega_H^2 P_2 P_3 P_5 (P_4 - \xi\pi_H),\\
Z_4 &= \pi_H \varphi r_2 P_5(\gamma\alpha\sigma + \psi P_3),\\
Z_5 &= \pi_H \omega_H r_2 P_5(\gamma\alpha\sigma + \psi P_3).
\end{aligned}
$$

Substituting (8) and (9) into the expression λ_R^{**} in (6), the resulting polynomial is

$$
\begin{aligned}
\mathcal{W}_R\left(\lambda_H^{**}, \lambda_R^{**}\right) = {} & U_1 \lambda_H^{**2} \lambda_R^{**3} + U_2 \lambda_H^{**2} \lambda_R^{**2} + U_3 \lambda_H^{**2} \lambda_R^{**} -\\
& U_4 \lambda_H^{**2} + U_5 \lambda_H^{**} \lambda_R^{**3} + U_6 \lambda_H^{**} \lambda_R^{**2} +\\
& U_7 \lambda_H^{**} \lambda_R^{**} - U_8 \lambda_H^{**} + U_9 \lambda_R^{**3} + U_{10} \lambda_R^{**2} +\\
& U_{11} \lambda_R^{**} = 0.
\end{aligned}
\tag{22}
$$

Where

$$
\begin{aligned}
U_1 &= \pi_R P_6 a_6,\\
U_2 &= \pi_R P_6(\omega_R a_6 + a_7) - \pi_R(\beta_R \eta a_6 + \beta_{eR} P_6 a_1),\\
U_3 &= \pi_R \omega_R P_6 a_7 - \pi_R(\beta_R \eta a_7 + \beta_{eR} P_6(\omega_R a_1 + a_2)),\\
U_4 &= \pi_R \omega_R \beta_{eR} P_6 a_2,\\
U_5 &= \pi_R P_6 a_8,\\
U_6 &= \pi_R P_6(\omega_R a_8 + a_9) - \pi_R(\beta_R \eta a_8 + \beta_{eR} P_6 a_3),\\
U_7 &= \pi_R \omega_R P_6 a_9 - \pi_R(\beta_R \eta a_9 + \beta_{eR} P_6(\omega_R a_3 + a_4)),\\
U_8 &= \pi_R \omega_R \beta_{eR} P_6 a_4,\\
U_9 &= \pi_R P_6 a_{10},\\
U_{10} &= \pi_R \omega_R P_6 a_{10}\left(1 - \mathscr{R}_0^R\right) + \pi_R P_6 a_{11}\left(1 - \mathscr{R}_0^{eR}\right),\\
U_{11} &= \pi_R \omega_R P_6 a_{11}\left(1 - \left(\mathscr{R}_0^R + \mathscr{R}_0^{eR}\right)\right).
\end{aligned}
$$

By adding the polynomial $\mathcal{W}_H\left(\lambda_H^{**}, \lambda_R^{**}\right)$ in (21) and the polynomial $\mathcal{W}_R\left(\lambda_H^{**}, \lambda_R^{**}\right)$ in (22), we obtained

$$
\begin{aligned}
\mathcal{W}_{HR}\left(\lambda_H^{**}, \lambda_R^{**}\right) = {} & \Theta_1 \lambda_H^{**5} \lambda_R^{**2} + \Theta_2 \lambda_H^{**5} \lambda_R^{**} + \Theta_3 \lambda_H^{**5} +\\
& \Theta_4 \lambda_H^{**4} \lambda_R^{**2} + \Theta_5 \lambda_H^{**4} \lambda_R^{**} + \Theta_6 \lambda_H^{**4} +\\
& \Theta_7 \lambda_H^{**3} \lambda_R^{**2} + \Theta_8 \lambda_H^{**3} \lambda_R^{**} + \Theta_9 \lambda_H^{**3} +\\
& U_1 \lambda_H^{**2} \lambda_R^{**3} + \left(\Theta_{10} + U_2\right) \lambda_H^{**2} \lambda_R^{**2} +\\
& \left(\Theta_{11} + U_3\right) \lambda_H^{**2} \lambda_R^{**} + \left(\Theta_{12} - U_4\right) \lambda_H^{**2} +\\
& U_5 \lambda_H^{**} \lambda_R^{**3} + \left(\Theta_{13} + U_6\right) \lambda_H^{**} \lambda_R^{**2} +\\
& \left(\Theta_{14} + U_7\right) \lambda_H^{**} \lambda_R^{**} + \left(\Theta_{15} - U_8\right) \lambda_H^{**} +\\
& U_9 \lambda_R^{**3} + \left(U_{10} - \Theta_{16}\right) \lambda_R^{**2} +\\
& \left(U_{11} - \Theta_{17}\right) \lambda_R^{**} = 0.
\end{aligned}
\tag{23}
$$

The nature of the polynomial $\mathcal{W}_{HR}\left(\lambda_H^{**}, \lambda_R^{**}\right)$ is indicative of the backward bifurcation phenomenon.

Chances of Backward Bifurcation Existence

The potential for backward bifurcation is investigated through the Center Manifold Theory, a method extensively developed and applied by Castillo-Chavez and Song (Castillo-Chavez and Song 2004).

Castillo-Chavez and Song theorem

Theorem 4. *Assume a general system of ordinary differential equations, influenced by the parameter ϑ;*

$$
\frac{dz}{dt} = h\left(z, \vartheta\right), h : \mathbb{R}^n \times \mathbb{R} \to \mathbb{R}^n, h \in \mathbf{C}^2\left(\mathbb{R}^n \times \mathbb{R}\right), \tag{24}
$$

where the system's equilibrium point in equation (24) is $z = 0$. In other words, $h\left(0, \vartheta\right) \equiv 0 \; \forall \; \vartheta$. Consider the following assumptions:

$\mathscr{G}_1$: The linearisation of the system about the equilibrium at the origin, given by equation (24), is represented by the matrix $A = D_z h\left(0, 0\right) = \left[\frac{\partial h}{\partial z}\left(0, 0\right)\right]$, where ϑ is evaluated at zero. This matrix has a simple eigenvalue at zero, and all other eigenvalues lie in the left half of the complex plane, indicating they have negative real parts.

$\mathscr{G}_2$: Corresponding to the zero eigenvalue of A, the matrix admits a left eigenvector v and a right eigenvector w, where w is

non-negative. Let h_k be the k^{th} component of h and

$$\begin{aligned}\mathcal{O}_a &= \sum_{k,i,j=1}^{n} v_k w_i w_j \frac{\partial^2 h_k}{\partial z_i \partial z_j}(0,0),\\ \mathcal{O}_b &= \sum_{k,i=1}^{n} v_k w_i \frac{\partial^2 h_k}{\partial z_i \partial \vartheta}(0,0).\end{aligned} \tag{25}$$

The local dynamics of equation (24) in the vicinity of the equilibrium point 0 are entirely dictated by the signs of of $\mathcal{O}_a$ and $\mathcal{O}_b$.

1. In the case where both $\mathcal{O}_a > 0$ and $\mathcal{O}_b > 0$,
   (i) For $\vartheta < 0$ with $|\vartheta| \ll 1$, the system admits a positive unstable equilibrium, while the equilibrium at the origin is locally asymptotically stable.
   (ii) In the regime where $0 < \vartheta \ll 1$, a negative locally asymptotically stable equilibrium emerges, and the equilibrium at zero loses stability.
2. If both $\mathcal{O}_a < 0$ and $\mathcal{O}_b < 0$:
   (i) When $\vartheta < 0$ and $|\vartheta| \ll 1$, the equilibrium at the origin is unstable.
   (ii) In the regime $0 < \vartheta \ll 1$, the origin remains locally asymptotically stable, and a positive unstable equilibrium emerges.
3. If $\mathcal{O}_a > 0$ and $\mathcal{O}_b < 0$:
   (i) When $\vartheta < 0$ with $|\vartheta| \ll 1$, the system possesses a locally asymptotically stable negative equilibrium, while the equilibrium at the origin is unstable.
   (ii) When $0 < \vartheta \ll 1$, a positive unstable equilibrium emerges, while the equilibrium at the origin remains locally asymptotically stable.
4. Under the conditions $\mathcal{O}_a < 0$ and $\mathcal{O}_b > 0$, a change in ϑ from negative to positive causes a stability shift at the origin, from stable to unstable, and gives rise to a positive, locally asymptotically stable equilibrium, while the previously existing negative equilibrium becomes unstable or disappears.

The type of bifurcation is determined by the signs of the coefficients: it is forward when $\mathcal{O}_a < 0$ and $\mathcal{O}_b > 0$, and backward when $\mathcal{O}_a > 0$ and $\mathcal{O}_b > 0$. Employing this approach allows us to establish the corresponding theorem.

Theorem 5. *The Mpox model (1) undergoes backward bifurcation at* $\mathscr{R}_0^M = 1$.

Proof. We use center manifold theory (Castillo-Chavez and Song 2004) to examine the bifurcation's nature. The following change of variables must be introduced for this theory to be applied effectively: Let $S_H = z_1$, $E_H = z_2$, $Q = z_3$, $I_H = z_4$, $T_H = z_5$, $R_H = z_6$, $S_R = z_7$, $E_R = z_8$, $I_R = z_9$, and $M = z_{10}$. So that

$$N_H = \sum_{i=1}^{6} z_i \quad and \quad N_R = \sum_{i=7}^{9} z_i$$

Additionally, by introducing the vector notation $z = (z_1, z_2, z_3, ..., z_{10})^T$ and $\frac{dz}{dt} = H(z)$, where $H = (h_1, h_2, h_3, ..., h_{10})^T$, the Mpox model (1) can be equivalently expressed as:

$$\begin{aligned}
\frac{dz_1}{dt} &\equiv h_1 = (1-\xi z_4)\pi_H - \lambda_H z_1 - \omega_H z_1 + (1-\alpha)\sigma z_3,\\
\frac{dz_2}{dt} &\equiv h_2 = \lambda_H z_1 - (\gamma + \psi + \omega_H) z_2,\\
\frac{dz_3}{dt} &\equiv h_3 = \gamma z_2 - (\sigma + \omega_H) z_3,\\
\frac{dz_4}{dt} &\equiv h_4 = \psi z_2 + \alpha\sigma z_3 + \xi \pi_H z_4 + \varphi \lambda_H z_6 - (\tau + \delta_H + \omega_H) z_4,\\
\frac{dz_5}{dt} &\equiv h_5 = \tau z_4 - (\theta + \phi\delta_H + \omega_H) z_5,\\
\frac{dz_6}{dt} &\equiv h_6 = \theta z_5 - (\varphi \lambda_H + \omega_H) z_6,\\
\frac{dz_7}{dt} &\equiv h_7 = \pi_R - \lambda_R z_7 - \omega_R z_7,\\
\frac{dz_8}{dt} &\equiv h_8 = \lambda_R z_7 - (\eta + \omega_R) z_8,\\
\frac{dz_9}{dt} &\equiv h_9 = \eta z_8 - \omega_R z_9,\\
\frac{dz_{10}}{dt} &\equiv h_{10} = r_1 z_9 + r_2 z_4 - \omega_e z_{10}.
\end{aligned} \tag{26}$$

Where

$$\lambda_H = \frac{\beta_H z_4 + \beta_{RH} z_9}{z_1 + z_2 + z_3 + z_4 + z_5 + z_6} + \frac{\beta_{eH} z_{10}}{K + z_{10}}, and$$

$$\lambda_R = \frac{\beta_R z_9}{z_7 + z_8 + z_9} + \frac{\beta_{eR} z_{10}}{K + z_{10}}.$$

We considered the transmission rate β_H to be the bifurcation parameter. Upon determining $\beta_H = \beta_H^*$ from $\mathscr{R}_0^M = 1$, we obtained

$$\begin{aligned}
\beta_H^* = {} & \frac{K\omega_H\omega_R^2\omega_e P_2 P_3 P_6 (P_4 - \xi\pi_H)}{(\gamma\alpha\sigma + \psi P_3)\left(K\omega_H\omega_R\omega_e(\omega_R P_6 - \beta_R\eta) - \beta_{eR}\eta\pi_R\omega_H r_1\right)}\\
& + \frac{r_2\left(\beta_R\beta_{eH}\pi_H\omega_R\eta - \beta_{eR}\beta_{RH}\pi_R\omega_H\eta - \beta_{eH}\pi_H\omega_R^2 P_6\right)}{K\omega_H\omega_R^2\omega_e P_6 - \eta(\beta_{eR}\pi_R\omega_H r_1 - \beta_R K\omega_H\omega_R\omega_e)} -\\
& \frac{\omega_H\eta P_2 P_3\left(\beta_R\omega_R\omega_e K + \beta_{eR}\pi_R r_1\right)(P_4 - \xi\pi_H)}{(\gamma\alpha\sigma + \psi P_3)\left(K\omega_H\omega_R\omega_e(\omega_R P_6 - \beta_R\eta) - \beta_{eR}\eta\pi_R\omega_H r_1\right)}
\end{aligned} \tag{27}$$

The Jacobian matrix of the modified system (26) at the Mpox disease-free equilibrium (ℓ_0) when $\beta_H = \beta_H^*$, is represented by:

$$\mathcal{J}(\ell_0)|_{\beta_H = \beta_H^*} =$$

$$\begin{bmatrix}
-\omega_H & 0 & P_1 & -\Psi_1 & 0 & 0 & 0 & 0 & -\beta_{RH} & -\Psi_3\\
0 & -P_2 & 0 & \beta_H & 0 & 0 & 0 & 0 & \beta_{RH} & \Psi_3\\
0 & \gamma & -P_3 & 0 & 0 & 0 & 0 & 0 & 0 & 0\\
0 & \psi & \alpha\sigma & \Psi_2 & 0 & 0 & 0 & 0 & 0 & 0\\
0 & 0 & 0 & \tau & -P_5 & 0 & 0 & 0 & 0 & 0\\
0 & 0 & 0 & 0 & \theta & -\omega_H & 0 & 0 & 0 & 0\\
0 & 0 & 0 & 0 & 0 & 0 & -\omega_R & 0 & -\beta_R & -\Psi_4\\
0 & 0 & 0 & 0 & 0 & 0 & 0 & -P_6 & \beta_R & \Psi_4\\
0 & 0 & 0 & 0 & 0 & 0 & 0 & \eta & -\omega_R & 0\\
0 & 0 & 0 & r_2 & 0 & 0 & 0 & 0 & r_1 & -\omega_e
\end{bmatrix}$$

where

$P_1 = (1-\alpha)\sigma$, $P_2 = \gamma + \psi + \omega_H$, $P_3 = \sigma + \omega_H$, $P_4 = \tau + \delta_H + \omega_H$, $P_5 = \theta + \phi\delta_H + \omega_H$, $P_6 = \eta + \omega_R$, $\Psi_1 = (\beta_H + \xi\pi_H)$, $\Psi_2 = \xi\pi_H - P_4$, $\Psi_3 = \frac{\beta_{eH}\pi_H}{K\omega_H}$, and $\Psi_4 = \frac{\beta_{eR}\pi_R}{K\omega_R}$. Let $w = (w_1, w_2, w_3, w_4, w_5, w_6, w_7, w_8, w_9, w_{10})^T$ denote the right eigenvector associated with the simple zero eigenvalue. It can be obtained by solving $\mathcal{J}(\ell_0)|_{\beta_H=\beta_B^*} w = 0$, and is represented as follows:

$$
\begin{aligned}
&-\omega_H w_1 + P_1 w_3 - (\beta_H^* + \xi\pi_H) w_4 - \beta_{RH} w_9 - \frac{\beta_{eH}\pi_H w_{10}}{K\omega_H} = 0,\\
&-P_2 w_2 + \beta_H^* w_4 + \beta_{RH} w_9 + \frac{\beta_{eH}\pi_H w_{10}}{K\omega_H} = 0,\\
&\gamma w_2 - P_3 w_3 = 0,\\
&\psi w_2 + \alpha\sigma w_3 + (\xi\pi_H - P_4) w_4 = 0,\\
&\tau w_4 - P_5 w_5 = 0,\\
&\theta w_5 - \omega_H w_6 = 0,\\
&-\omega_R w_7 - \beta_R w_9 - \frac{\beta_{eR}\pi_R w_{10}}{K\omega_R} = 0,\\
&-P_6 w_8 + \beta_R w_9 + \frac{\beta_{eR}\pi_R w_{10}}{K\omega_R} = 0,\\
&\eta w_8 - \omega_R w_9 = 0,\\
&r_2 w_4 + r_1 w_9 - \omega_e w_{10} = 0.
\end{aligned}
\tag{28}
$$

solving the above equation (28), we obtained

$$
\begin{aligned}
&w_1 = \frac{((P_1\gamma - P_2P_3)(P_4 - \xi\pi_H) - \xi\pi_H(P_3\psi + \gamma\alpha\sigma))\, w_2}{\omega_H P_3(P_4 - \xi\pi_H)},\\
&w_2 = w_2 > 0, w_3 = \frac{\gamma w_2}{P_3}, w_4 = \frac{(\psi P_3 + \gamma\alpha\sigma) w_2}{P_3(P_4 - \xi\pi_H)},\\
&w_5 = \frac{\tau(\psi P_3 + \gamma\alpha\sigma) w_2}{P_3 P_5(P_4 - \xi\pi_H)}, w_6 = \frac{\theta\tau(\psi P_3 + \gamma\alpha\sigma) w_2}{\omega_H P_3 P_5(P_4 - \xi\pi_H)},\\
&w_7 = -\frac{P_6 w_9}{\eta}, w_8 = \frac{\omega_R w_9}{\eta}, w_9 = w_9 > 0,\\
&w_{10} = \frac{r_1 P_3(P_4 - \xi\pi_H) w_9 + r_2(\psi P_3 + \gamma\alpha\sigma) w_2}{\omega_e P_3(P_4 - \xi\pi_H)}.
\end{aligned}
\tag{29}
$$

Similarly, the left eigenvector $v = (v_1, v_2, v_3, v_4, v_5, v_6, v_7, v_8, v_9, v_{10})$, corresponding to the simple zero eigenvalue and satisfying the normalization condition $v.w = 1$,can be determined by solving the equation $v\mathcal{J}(\ell_0)|_{\beta_H=\beta_B^*} = 0$, as follows

$$
\begin{aligned}
&-\omega_H v_1 = 0,\\
&-P_2 v_2 + \gamma v_3 + \psi v_4 = 0,\\
&P_1 v_1 - P_3 v_3 + \alpha\sigma v_4 = 0,\\
&-(\beta_H^* + \xi\pi_H) v_1 + \beta_H^* v_2 + (\xi\pi_H - P_4) v_4 + \tau v_5 + r_2 v_{10} = 0,\\
&-P_5 v_5 + \theta v_6 = 0,\\
&-\omega_H v_6 = 0,\\
&-\omega_R v_7 = 0,\\
&-P_6 v_8 + \eta v_9 = 0,\\
&-\beta_{RH} v_1 + \beta_{RH} v_2 - \beta_R v_7 + \beta_R v_8 - \omega_R v_9 + r_1 v_{10} = 0,\\
&-\frac{\beta_{eH}\pi_H v_1}{K\omega_H} + \frac{\beta_{eH}\pi_H v_2}{K\omega_H} - \frac{\beta_{eR}\pi_R v_7}{K\omega_R} + \frac{\beta_{eR}\pi_R v_8}{K\omega_R} - \omega_e v_{10} = 0
\end{aligned}
\tag{30}
$$

From (30), we obtained

$$
\begin{aligned}
&v_1 = v_5 = v_6 = v_7 = 0, v_2 = \frac{(\psi P_3 + \gamma\alpha\sigma) v_4}{P_2 P_3}, v_3 = \frac{\alpha\sigma v_4}{P_3},\\
&v_4 = v_4 > 0, v_8 = \frac{\eta v_9}{P_6}, v_9 = v_9 > 0,\\
&v_{10} = \frac{\beta_{eH}\pi_H(\psi P_3 + \gamma\alpha\sigma) v_4}{K\omega_e\omega_H P_2 P_3} + \frac{\beta_{eR}\pi_R\eta v_9}{K\omega_e\omega_R P_6}.
\end{aligned}
\tag{31}
$$

Determination of $\mathcal{O}_a$ and $\mathcal{O}_b$

Since $v_1 = 0, v_5 = 0, v_6 = 0$, and $v_7 = 0$ for each $k \in \{1, 2, 3, ..., 10\}$, the remaining non-zero partial derivatives are as follows:

$$
\begin{aligned}
&\frac{\partial^2 h_2}{\partial z_2 \partial z_4} = \frac{\partial^2 h_2}{\partial z_4 \partial z_2} = \frac{\partial^2 h_2}{\partial z_3 \partial z_4} = \frac{\partial^2 h_2}{\partial z_4 \partial z_3} = \frac{\partial^2 h_2}{\partial z_4 \partial z_5} = \frac{\partial^2 h_2}{\partial z_5 \partial z_4} =\\
&\frac{\partial^2 h_2}{\partial z_4 \partial z_6} = \frac{\partial^2 h_2}{\partial z_6 \partial z_4} = -\frac{\beta_H^* \omega_H}{\pi_H},\\
&\frac{\partial^2 h_2}{\partial z_2 \partial z_9} = \frac{\partial^2 h_2}{\partial z_9 \partial z_2} = \frac{\partial^2 h_2}{\partial z_3 \partial z_9} = \frac{\partial^2 h_2}{\partial z_9 \partial z_3} = \frac{\partial^2 h_2}{\partial z_4 \partial z_9} = \frac{\partial^2 h_2}{\partial z_9 \partial z_4} =\\
&\frac{\partial^2 h_2}{\partial z_5 \partial z_9} = \frac{\partial^2 h_2}{\partial z_9 \partial z_5} = -\frac{\beta_{RH}\omega_H}{\pi_H},\\
&\frac{\partial^2 h_2}{\partial z_6 \partial z_9} = \frac{\partial^2 h_2}{\partial z_9 \partial z_6} = -\frac{\beta_{RH}\omega_H}{\pi_H}, \frac{\partial^2 h_2}{\partial z_1 \partial z_{10}} = \frac{\partial^2 h_2}{\partial z_{10} \partial z_1} = \frac{\beta_{eH}}{K},\\
&\frac{\partial^2 h_8}{\partial z_8 \partial z_9} = \frac{\partial^2 h_8}{\partial z_9 \partial z_8} = -\frac{\beta_R \omega_R}{\pi_R},\\
&\frac{\partial^2 h_8}{\partial z_7 \partial z_{10}} = \frac{\partial^2 h_8}{\partial z_{10} \partial z_7} = \frac{\beta_{eR}}{K}, \frac{\partial^2 h_2}{\partial z_4^2} = -\frac{2\beta_H^* \omega_H}{\pi_H},\\
&\frac{\partial^2 h_8}{\partial z_9^2} = -\frac{2\beta_R \omega_R}{\pi_R}, \frac{\partial^2 h_2}{\partial z_4 \partial \beta_H^*} = 1
\end{aligned}
\tag{32}
$$

but

$$
\mathcal{O}_a = \sum_{k,i,j=1}^{n} v_k w_i w_j \frac{\partial^2 h_k}{\partial z_i \partial z_j}(0,0)
$$

$$
\begin{aligned}
\mathcal{O}_a = &-\frac{2v_4 w_2^2 \beta_H^* \omega_H (\psi P_3 + \gamma\alpha\sigma)^2 (P_3 + \gamma)}{\pi P_2 P_3^3 (P_4 - \xi\pi_H)} -\\
&\frac{2v_4 w_2^2 \beta_H^* \tau(\psi P_3 + \gamma\alpha\sigma)^3 (\theta + \mu_H)}{\pi P_2 P_3^3 P_5 (P_4 - \xi\pi_H)^2} -\\
&\frac{2v_4 w_2 w_9 \beta_{RH} \omega_H (\psi P_3 + \gamma\alpha\sigma)(P_3 + \gamma)}{\pi P_2 P_3^2} -\\
&\frac{2v_4 w_2 w_9 \beta_{RH} (\psi P_3 + \gamma\alpha\sigma)^2 (\tau(\theta + \mu_H) + \omega_H P_5)}{\pi P_2 P_3^2 P_5 (P_4 - \xi\pi_H)} -\\
&\frac{2v_9 w_9 \beta_{eR} (r_1 P_3 (P_4 - \xi\pi_H) w_9 + r_2(\psi P_3 + \gamma\alpha\sigma) w_2)}{K\omega_e P_3 (P_4 - \xi\pi_H)} -\\
&\frac{2v_9 w_9^2 \beta_R \omega_R (\eta + \omega_R)}{\pi_R P_6} +\\
&\frac{2v_4 w_2 w_9 \beta_{eH} r_1 (\psi P_3 + \gamma\alpha\sigma)(P_1\gamma - P_2 P_3)}{K\omega_H \omega_e P_2 P_3^2} -\\
&\frac{2v_4 w_2 w_9 \beta_{eH} r_1 \xi\pi_H (\psi P_3 + \gamma\alpha\sigma)^2}{K\omega_H \omega_e P_2 P_3^2 (P_4 - \xi\pi_H)} +\\
&\frac{2v_4 w_2^2 \beta_{eH} r_2 (\psi P_3 + \gamma\alpha\sigma)^2 (P_1\gamma - P_2 P_3)}{K\omega_H \omega_e P_2 P_3^3 (P_4 - \xi\pi_H)} -\\
&\frac{2v_4 w_2^2 \beta_{eH} r_2 \xi\pi_H (\psi P_3 + \gamma\alpha\sigma)^3}{K\omega_H \omega_e P_2 P_3^3 (P_4 - \xi\pi_H)^2} -\\
&\frac{2v_4 w_2^2 \beta_H^* \omega_H (\psi P_3 + \gamma\alpha\sigma)^3}{\pi_H P_2 P_3^3 (P_4 - \xi\pi_H)^2},
\end{aligned}
\tag{33}
$$

and

$$\mathcal{O}_b = \sum_{k,i=1}^{n} v_k w_i \frac{\partial^2 h_k}{\partial z_i \partial \vartheta}(0,0)$$

$$\mathcal{O}_b = \frac{v_4 w_2 (\psi P_3 + \gamma \alpha \sigma)^2}{P_2 P_3^2 (P_4 - \xi \pi_H)} > 0 \tag{34}$$

Thus, according to Theorem 5 in Castillo-Chavez and Song (2004), the Mpox model exhibits a backward bifurcation at $\mathscr{R}_0^M = 1$ when $\mathcal{O}_a > 0$, accompanied by a non-negative bifurcation coefficient $\mathcal{O}_b$. □

Epidemiological Interpretation of the Bifurcation Point

The center manifold analysis reveals that the system undergoes a backward bifurcation at $\mathscr{R}_0^M = 1$ if $a > 0$, indicating that this threshold does not guarantee disease elimination. Epidemiologically, this means that Mpox can persist in the population even when the basic reproduction number is reduced below unity, due to the coexistence of a stable disease-free equilibrium and a stable endemic equilibrium. Consequently, disease outcomes depend on initial levels of infection in the human population, rodent reservoir, and environmental viral concentration. This result underscores the importance of early and comprehensive control measures, as reducing $\mathscr{R}_0^M$ below one alone may be insufficient to eradicate Mpox without simultaneously lowering infection prevalence and environmental contamination.

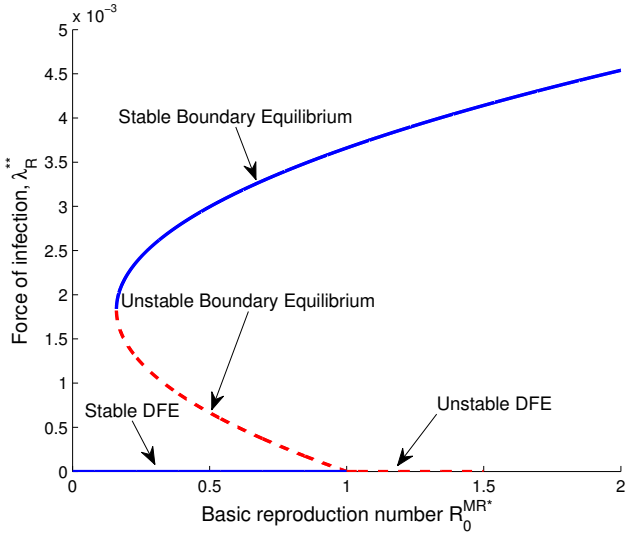

Figure 2 Bifurcation Diagram for the Rodent-only Boundary equilibrium of the Mpox model, with $\beta_R = 0.0077$ and $\beta_{eR} = 0.7$. The critical value of $\mathscr{R}_0^{MR*}$ is $\mathscr{R}_0^{MR*} = \mathscr{R}_c^{MR*} = 0.16$.

Figures 2 and 3 depict the phenomenon of bistability between the mpox disease-free equilibrium and the boundary (endemic) equilibrium in the proposed model. The presence of a backward bifurcation suggests the coexistence of a locally stable disease-free equilibrium and a stable boundary endemic equilibrium, even when the basic reproduction numbers for both the human and rodent populations are less than one. Figures 2 and 3 were obtained by numerically simulating the polynomials $\mathscr{L}(\lambda_R^{**})$ and $\mathscr{T}(\lambda_H^{**})$ in equations (13) and (17), using the parameter values $\beta_R = 0.0077$, $\beta_H = 0.18$, $\beta_{eR} = 0.7$, $\psi = 0.6744$, and the remaining parameter values from Table 2 and 3 to determine the possible number of positive roots. It is shown that, although the associated basic reproduction numbers ($\mathscr{R}_0^{MR*}$ and $\mathscr{R}_0^{MH*}$) are less than one, and the

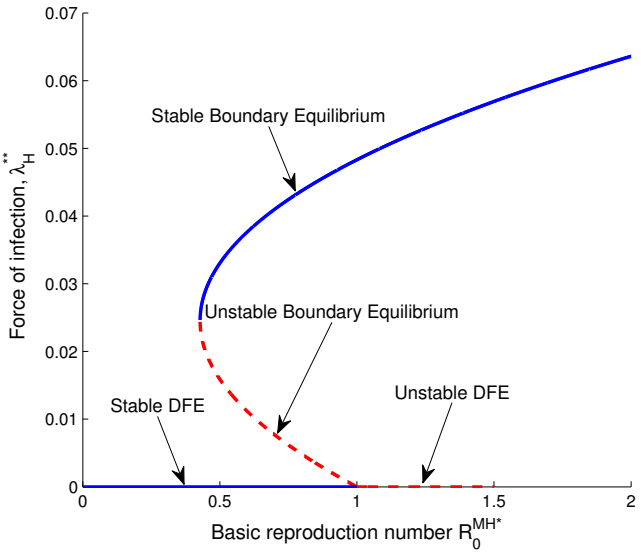

Figure 3 Bifurcation Diagram for the Human-only Boundary equilibrium of the Mpox model, with $\beta_H = 0.18$ and $\psi = 0.6744$, The critical value of $\mathscr{R}_0^{MH*}$ is $\mathscr{R}_0^{MH*} = \mathscr{R}_c^{MH*} = 0.43$.

disease-free equilibrium is stable, there might still be another stable boundary (endemic) equilibrium that coexists simultaneously. This means that even if the associated basic reproduction numbers are less than one, a population may still resides at an endemic (boundary) equilibrium at which the Mpox persists indefinitely. In Figure 2, it is important to note that three equilibria coexist when $\mathscr{R}_0^{MR*}$ lies within the range $0 < \mathscr{R}_c^{MR*} < \mathscr{R}_0^{MR*} < 1$ (where $\mathscr{R}_c^{MR*}$ is the critical value, $\mathscr{R}_c^{MR*} = 0.16$). These equilibria include a stable disease-free equilibrium, an unstable boundary equilibrium, and a stable boundary equilibrium. Thus, when $\mathscr{R}_0^{MR*} < \mathscr{R}_c^{MR*}$, only the stable disease-free equilibrium exists. Similarly, in Figure 3, when $\mathscr{R}_0^{MH*}$ falls within the range $0 < \mathscr{R}_c^{MH*} < \mathscr{R}_0^{MH*} < 1$ (with $\mathscr{R}_c^{MH*}$ being the critical value and $\mathscr{R}_c^{MH*} = 0.43$), a stable disease-free equilibrium, an unstable boundary equilibrium, and a stable boundary equilibrium coexist. Therefore, when $\mathscr{R}_0^{MH*} < \mathscr{R}_c^{MH*}$, only the stable disease-free equilibrium exists.

Biologically, the implication of backward bifurcation is that when the associated basic reproduction numbers ($\mathscr{R}_0^{MR*}$ and $\mathscr{R}_0^{MH*}$) exceed one, reducing them to below one is no longer sufficient to guarantee the elimination of Mpox. In the proposed Mpox model, this phenomenon occurs because;

1. Multiple infection sources (direct human-to-human transmission, rodent to human spillover, and environment-mediated transmission) allow the virus to persist even when each individual pathway is weak.

2. Environmental persistence of MPXV creates a memory effect in the system where by past infections continue to influence current transmission through contaminated surfaces or materials.

3. Rodent reservoir dynamics sustain low-level infection that can continuously re-introduce the virus into the human population, preventing extinction at low reproduction numbers.

4. Nonlinear incidence and feedback between host and environment compartments introduce strong coupling effects that

generate multiple endemic equilibria.

Hence, backward bifurcation in this Mpox model reflects the biological reality that Mpox control requires more than threshold reduction, necessitating simultaneous interventions targeting human transmission, rodent reservoirs, and environmental decontamination.

Uncertainty and Sensitivity Analysis

The effects of model parameters on the spread and progression of Mpox shall be examined through uncertainty and sensitivity analyses based on Latin Hypercube Sampling (LHS) and Partial Rank Correlation Coefficient (PRCC) (Gumel *et al.* 2018). LHS is a statistical sampling technique that efficiently explores the parameter space by generating a large number of parameter combinations that span the full range of each parameter while ensuring that all regions of the parameter space are adequately represented. This approach allows modelers to account for natural variability and uncertainty in parameter estimates without the need for exhaustive simulations of all possible parameter combinations. The sampled parameter sets are used to simulate the model, and the resulting output, specifically the basic reproduction number ($\mathscr{R}_0^M$), is analyzed to determine which parameters exert the greatest influence on model outcomes. Following the simulations, PRCC analysis is applied to quantify the relative influence of each parameter on the model output while controlling for the effects of all other parameters. PRCC measures the strength and direction of monotonic relationships between input parameters and model outputs, making it particularly suitable for nonlinear and complex dynamical systems. The combined LHS and PRCC framework not only identifies the parameters that most strongly contribute to uncertainty in the model output but also highlights those parameters for which accurate estimation is critical. As such, this approach provides valuable guidance for future data collection efforts and the design of effective intervention strategies.

For each LHS run, a total of 1,000 simulations of the Mpox model (1) were conducted using biologically plausible ranges for the twenty-one parameters appearing in the expression for the basic reproduction number ($\mathscr{R}_0^M$). Parameters with PRCC values greater than 0.5 or less than -0.5 were classified as highly influential, indicating that small variations in these parameters can lead to substantial changes in model predictions. In general, PRCC values approaching -1 or $+1$ indicate a strong influence of the associated model parameter on $\mathscr{R}_0^M$. A negative PRCC value indicates an inverse relationship with the response function, whereas a positive value reflects a direct relationship (Gumel *et al.* 2018). The sensitivity analysis results of the Mpox model (1), using $\mathscr{R}_0^M$ as the response function, reveal (as shown in Table 4 and Figure 4) that the top-ranked parameters positively correlated with $\mathscr{R}_0^M$ are the transmission rate between infected and susceptible humans (β_H), the transmission rate between infected and susceptible rodents (β_R), and the proportion of quarantined humans who progress to the infected class (α). Increases in these parameters lead to higher values of $\mathscr{R}_0^M$. Conversely, the parameters most strongly negatively correlated with $\mathscr{R}_0^M$ are the treatment rate of infected humans (τ), the rodent death rate (ω_R), and the natural death rate of humans (ω_H). Increases in these parameters result in a reduction of the basic reproduction number.

EXTENSION OF THE MODEL WITH CONTROL STRATEGIES

To highlight the critical role of community education, public awareness, and enlightenment campaigns in curbing the transmission

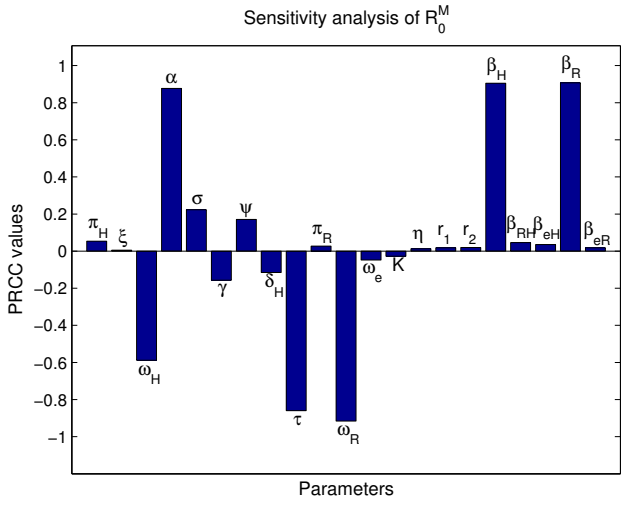

Figure 4 Partial rank correlation coefficient (PRCC) bar chart showing the sensitivity of $\mathscr{R}_0^M$ to the model parameters.

of Mpox, two time-dependent control strategies were incorporated into the Mpox model (1). The first control captures the preventive measures adopted by susceptible individuals to reduce the risk of infection. These precautionary behaviors, represented by $u_1(t) \in [0,1]$, include regular handwashing, the use of gloves when handling rodents, and avoiding direct contact with the open lesions of infected individuals. The second control, denoted by $u_2(t) \in [0,1]$, involves the application of disinfectants (e.g., for laundering clothes and cleaning surfaces) and adherence to proper sanitation practices aimed at accelerating the decay rate of MPXV in the environment. With the integration of these two time-dependent control measures, the Mpox model (1) is reformulated as follows:

$$
\begin{aligned}
\frac{dS_H}{dt} &= (1-\xi I_H)\,\pi_H - (1-u_1(t))\lambda_H S_H - \omega_H S_H + (1-\alpha)\,\sigma Q,\\
\frac{dE_H}{dt} &= (1-u_1(t))\lambda_H S_H - (\gamma+\psi+\omega_H)\,E_H,\\
\frac{dQ}{dt} &= \gamma E_H - (\sigma+\omega_H)\,Q,\\
\frac{dI_H}{dt} &= \psi E_H + \alpha\sigma Q + \xi\pi_H I_H + (1-u_1(t))\varphi\lambda_H R_H -\\
&\quad (\tau+\delta_H+\omega_H)\,I_H,\\
\frac{dT_H}{dt} &= \tau I_H - (\theta+\phi\delta_H+\omega_H)\,T_H,\\
\frac{dR_H}{dt} &= \theta T_H - ((1-u_1(t))\varphi\lambda_H+\omega_H)\,R_H,\\
\frac{dS_R}{dt} &= \pi_R - \lambda_R S_R - \omega_R S_R,\\
\frac{dE_R}{dt} &= \lambda_R S_R - (\eta+\omega_R)\,E_R,\\
\frac{dI_R}{dt} &= \eta E_R - \omega_R I_R,\\
\frac{dM}{dt} &= r_1 I_R + r_2 I_H - (\omega_e + u_2(t))M.
\end{aligned}
\tag{35}
$$

Where

$$
\lambda_H = \frac{\beta_H I_H + \beta_{RH} I_R}{N_H} + \frac{\beta_{eH} M}{K+M}, \text{and} \quad \lambda_R = \frac{\beta_R I_R}{N_R} + \frac{\beta_{eR} M}{K+M}.
$$

Table 4 PRCC analysis of the response function $\mathscr{R}_0^M$ for all model input parameters

Input parameter	Parameter range	PRCC ($\mathscr{R}_0^M$)
π_H	[0.02746, 0.04576]	0.0538
ξ	$[7.5 \times 10^{-9}, 1.25 \times 10^{-8}]$	0.0048
ω_H	[0.00932, 0.01554]	-0.5879
α	[0.225, 0.375]	0.8766
σ	[0.075, 0.125]	0.2231
γ	[0.3, 0.5]	-0.1565
ψ	[0.012558, 0.02093]	0.1708
δ_H	[0.0024645, 0.0041075]	-0.1149
τ	[0.0375, 0.0625]	-0.8600
π_R	[0.15, 0.0025]	0.0270
ω_R	[0.0015, 0.0025]	-0.9156
ω_e	[0.2625, 0.4375]	-0.0476
K	[7500, 12500]	-0.0275
η	[0.255, 0.425]	0.0128
r_1	[0.075, 0.125]	0.0176
r_2	[0.0525, 0.0875]	0.0193
β_H	[0.02505, 0.04175]	0.9048
β_{RH}	[0.003935, 0.006558]	0.0461
β_{eH}	$[1.8676 \times 10^{-8}, 3.1126 \times 10^{-8}]$	0.0355
β_R	[0.000225, 0.000375]	0.9074
β_{eR}	$[7.5 \times 10^{-9}, 1.25 \times 10^{-8}]$	0.0183

Accordingly, we define the following objective functional:

$$\mathcal{J}[u_1, u_2] = \int_0^{t_f} \left[\mathscr{B}_1 I_H + \frac{1}{2} \left(\mathscr{B}_2 u_1^2(t) + \mathscr{B}_3 u_2^2(t) \right) \right] dt \qquad (36)$$

Here, t_f denotes the final time, and $\mathscr{B}_1$, $\mathscr{B}_2$, and $\mathscr{B}_3$ are the weight function to help balance the intergrand (36) so that no term will dominate the other. The term $\mathscr{B}_1 I_H$ quantifies the cost associated with monitoring infected humans at all stages, while $\mathscr{B}_2 u_1^2(t) + \mathscr{B}_3 u_2^2(t)$ represents the expenses incurred in implementing the control strategies.The objective is to minimize both the number of infected individuals and the overall cost. To achieve this, we aim to determine an optimal control pair $u_1(t)$ and $u_2(t)$ that satisfies:

$$\mathcal{J}[u_1^*, u_2^*] = \min_{u_1, u_2 \in \mathcal{D}} \mathcal{J}[u_1, u_2] \qquad (37)$$

where the admissible control set ($\mathcal{D}$) is defined by

$$\mathcal{D} = \Big\{ (u_1(t), u_2(t)) \in \mathscr{L}^1(0, t_f) \times \mathscr{L}^1(0, t_f) | a_1 \leq u_1(t) \geq b_1, \\ a_2 \leq u_2(t) \geq b_2 \} \qquad (38)$$

with each control function being Lebesgue measurable over the interval $[0, t_f]$.

Analysis of the Extended Model with Controls

Pontryagin's Maximum Principle (Pontryagin 2018) is employed to derive the necessary conditions for optimal control. Utilizing this principle, the system described by equations (35) and the objective functional (36) are reformulated into an optimization problem aimed at minimizing the Hamiltonian $\mathcal{H}$ with respect to the control variables $u_1(t)$ and $u_2(t)$ at each instant in time. To establish the optimality conditions, the Hamiltonian is first

constructed by combining the objective functional (36) with the system dynamics (35), yielding the following expressions:

$$\begin{aligned}\mathcal{H} &= \mathscr{B}_1 I_H + \frac{1}{2}\left(\mathscr{B}_2 u_1^2(t) + \mathscr{B}_3 u_2^2(t)\right) + \\ &\Lambda_1\left[(1-\xi I_H)\,\pi_H - (1-u_1(t))\left(\frac{\beta_H I_H + \beta_{RH} I_R}{N_H} + \frac{\beta_{eH} M}{K+M}\right) S_H\right. \\ &\left. -\omega_H S_H + (1-\alpha)\,\sigma Q\right] + \\ &\Lambda_2\left[(1-u_1(t))\left(\frac{\beta_H I_H + \beta_{RH} I_R}{N_H} + \frac{\beta_{eH} M}{K+M}\right) S_H -\right. \\ &\left.(\gamma+\psi+\omega_H)\,E_H\right] + \Lambda_3\left[\gamma E_H - (\sigma+\omega_H)\,Q\right] + \\ &\Lambda_4\left[\psi E_H + \alpha\sigma Q + \xi\pi_H I_H - (\tau+\delta_H+\omega_H)\,I_H + \right. \\ &\left.(1-u_1(t))\varphi\left(\frac{\beta_H I_H + \beta_{RH} I_R}{N_H} + \frac{\beta_{eH} M}{K+M}\right) R_H\right] \\ &+ \Lambda_5\left[\tau I_H - (\theta+\phi\delta_H+\omega_H)\,T_H\right] + \Lambda_6\left[\theta T_H -\right. \\ &\left.\left((1-u_1(t))\varphi\left(\frac{\beta_H I_H + \beta_{RH} I_R}{N_H} + \frac{\beta_{eH} M}{K+M}\right) + \omega_H\right) R_H\right] \\ &+ \Lambda_7\left[\pi_R - \left(\frac{\beta_R I_R}{N_R} + \frac{\beta_{eR} M}{K+M}\right) S_R - \omega_R S_R\right] + \\ &\Lambda_8\left[\left(\frac{\beta_R I_R}{N_R} + \frac{\beta_{eR} M}{K+M}\right) S_R - (\eta+\omega_R)\,E_R\right] + \\ &\Lambda_9\left[\eta E_R - \omega_R I_R\right] + \Lambda_{10}\left[r_1 I_R + r_2 I_H - (\omega_e + u_2(t))M\right]\end{aligned} \tag{39}$$

Here $\Lambda_1, \Lambda_2, \Lambda_3, \Lambda_4, \Lambda_5, \Lambda_6, \Lambda_7, \Lambda_8, \Lambda_9, \Lambda_{10}$ denote the adjoint functions associated with the state variables S_H, E_H, Q, I_H, T_H, R_H, S_R, E_R, I_R, and M, respectively. The associated system of adjoint equations is derived by taking the partial derivatives of the Hamiltonian (39) with respect to both the state and control variables.

Theorem 6. *The control pair u_1^* and u_2^*, and the solutions S_H^*, E_H^*, Q^*, I_H^*, T_H^*, R_H^*, S_R^*, E_R^*, I_R^*, M^* of the corresponding state system (35) that minimizes $\mathcal{J}[u_1, u_2]$ over $\mathcal{D}$, then there exists adjoint functions $\Lambda_1, \Lambda_2, \Lambda_3, \Lambda_4, \Lambda_5, \Lambda_6, \Lambda_7, \Lambda_8, \Lambda_9, \Lambda_{10}$, such that*

$$\begin{aligned}&\frac{d\Lambda_1}{dt} = \mathscr{C}_1, \frac{d\Lambda_2}{dt} = \mathscr{C}_2, \frac{d\Lambda_3}{dt} = \mathscr{C}_3, \frac{d\Lambda_4}{dt} = \mathscr{C}_4, \frac{d\Lambda_5}{dt} = \mathscr{C}_5, \\ &\frac{d\Lambda_6}{dt} = \mathscr{C}_6, \frac{d\Lambda_7}{dt} = \mathscr{C}_7, \frac{d\Lambda_8}{dt} = \mathscr{C}_8, \frac{d\Lambda_9}{dt} = \mathscr{C}_9, \frac{d\Lambda_{10}}{dt} = \mathscr{C}_{10}.\end{aligned} \tag{40}$$

The definitions of $\mathscr{C}_1, \mathscr{C}_2, \mathscr{C}_3, \mathscr{C}_4, \mathscr{C}_5, \mathscr{C}_6, \mathscr{C}_7, \mathscr{C}_8, \mathscr{C}_9$, and $\mathscr{C}_{10}$ are listed in the Appendix section.
In addition, the transversality conditions can be stated as:

$$\Lambda_i(t_f) = 0, \quad i = 1, 2, 3, ..., 10. \tag{41}$$

The subsequent characterization is valid;

$$\begin{aligned}u_1^* &= \max\left\{0, \min\left(1, \frac{\lambda_H\left((\Lambda_2-\Lambda_1)S_H + (\Lambda_4-\Lambda_6)\varphi R_H\right)}{\mathscr{B}_2}\right)\right\}, \\ u_2^* &= \max\left\{0, \min\left(1, \frac{\Lambda_{10} M}{\mathscr{B}_3}\right)\right\}\end{aligned} \tag{42}$$

where

$$\lambda_H = \left(\frac{\beta_H I_H + \beta_{RH} I_R}{N_H} + \frac{\beta_{eH} M}{K+M}\right).$$

Preposition 1. *According to Corollary 4.2 of Fleming and Rishel (1975) (Fleming and Rishel 2012), the existence of an optimal control pair $(u_1(t), u_2(t))$ is guaranteed under the conditions that the integrand of the objective functional $\mathcal{J}$ is convex with respect to the control variables, the state solutions remain bounded, and the model system (35) is locally Lipschitz continuous with respect to its state variables.*

Proof. Following Pontryagin's Maximum Principle, we have obtained:

$$\begin{aligned}\frac{d\Lambda_1}{dt} &= -\frac{\partial \mathcal{H}}{\partial S_H}, \quad \Lambda_1(t_f) = 0, \\ \frac{d\Lambda_2}{dt} &= -\frac{\partial \mathcal{H}}{\partial E_H}, \quad \Lambda_2(t_f) = 0, \\ \frac{d\Lambda_3}{dt} &= -\frac{\partial \mathcal{H}}{\partial Q}, \quad \Lambda_3(t_f) = 0, \\ \frac{d\Lambda_4}{dt} &= -\frac{\partial \mathcal{H}}{\partial I_H}, \quad \Lambda_4(t_f) = 0, \\ \frac{d\Lambda_5}{dt} &= -\frac{\partial \mathcal{H}}{\partial T_H}, \quad \Lambda_5(t_f) = 0, \\ \frac{d\Lambda_6}{dt} &= -\frac{\partial \mathcal{H}}{\partial R_H}, \quad \Lambda_6(t_f) = 0, \\ \frac{d\Lambda_7}{dt} &= -\frac{\partial \mathcal{H}}{\partial S_R}, \quad \Lambda_7(t_f) = 0, \\ \frac{d\Lambda_8}{dt} &= -\frac{\partial \mathcal{H}}{\partial E_R}, \quad \Lambda_8(t_f) = 0, \\ \frac{d\Lambda_9}{dt} &= -\frac{\partial \mathcal{H}}{\partial I_R}, \quad \Lambda_9(t_f) = 0, \\ \frac{d\Lambda_{10}}{dt} &= -\frac{\partial \mathcal{H}}{\partial M}, \quad \Lambda_{10}(t_f) = 0,\end{aligned} \tag{43}$$

and taking the optimality conditions into account;

$$\frac{\partial \mathcal{H}}{\partial u_1} = 0, and \quad \frac{\partial \mathcal{H}}{\partial u_2} = 0. \tag{44}$$

The optimal control functions $u_1(t)$ and $u_2(t)$ can be expressed in terms of the state variables. Taking into account the constraints on the control variables, the optimal controls are characterized as follows:

For $u_1(t)$, we have

$$\begin{aligned}\frac{\partial \mathcal{H}}{\partial u_1} &= u_1 \mathscr{B}_2 - (\Lambda_2 - \Lambda_1)\left(\frac{\beta_H I_H + \beta_{RH} I_R}{N_H} + \frac{\beta_{eH} M}{K+M}\right) S_H \\ &- (\Lambda_4 - \Lambda_6)\varphi\left(\frac{\beta_H I_H + \beta_{RH} I_R}{N_H} + \frac{\beta_{eH} M}{K+M}\right) R_H = 0\end{aligned} \tag{45}$$

Solving the right hand side of (45), we obtained

$$\begin{aligned}u_1^*(t) = &\frac{1}{\mathscr{B}_2}\left(\left(\frac{\beta_H I_H + \beta_{RH} I_R}{N_H} + \frac{\beta_{eH} M}{K+M}\right)(\Lambda_2 - \Lambda_1) S_H + \right. \\ &\left.\left(\frac{\beta_H I_H + \beta_{RH} I_R}{N_H} + \frac{\beta_{eH} M}{K+M}\right)(\Lambda_4 - \Lambda_6)\varphi R_H\right).\end{aligned} \tag{46}$$

For $u_2(t)$, we get

$$\frac{\partial \mathcal{H}}{\partial u_2} = u_2 \mathscr{B}_3 - \Lambda_{10} M, \tag{47}$$

which yields

$$u_2^*(t) = \frac{\Lambda_{10} M}{\mathscr{B}_3}. \tag{48}$$

Differentiation of the Hamiltonian with respect to the control variables yields the optimality conditions, valid throughout the interior of the admissible control set, concluding the proof. □

Numerical Simulation

The optimal control solution is obtained through the forward-backward sweep method, an iterative procedure initiated with an initial guess for the control functions. The state equations are first integrated forward in time using the fourth-order Runge-Kutta method. Subsequently, the computed state variables, together with the initial control estimates, are employed to solve the adjoint equations (40) by integrating backward in time from prescribed terminal conditions, also using the fourth-order Runge-Kutta scheme. Following this, the control functions $u_1(t)$ and $u_2(t)$ are updated based on the newly calculated state and adjoint variables.

This iterative process continues until convergence is achieved for the state, adjoint, and control variables, consistent with methodologies reported in prior works (Lenhart and Workman 2007; Kang *et al.* 2024; Oguntolu *et al.* 2025; Jose *et al.* 2022; Omede *et al.* 2023a). The initial condition used for the state variables are $S_H = 217000000$, $E_H = 5000$, $Q = 100$, $I_H = 50$, $T_H = 10$, $R_H = 0$, $S_R = 6000$, $E_R = 800$, $I_R = 80$, $M = 100$. The values of the weight function used are given by $\mathscr{B}_1 = 1$, $\mathscr{B}_2 = 0.5$, and $\mathscr{B}_3 = 0.10$. Furthermore, the parameter values used are $\beta_{eR} = 0.00001$, $\beta_{eH} = 0.000024901$ and the remaining parameter values are the same in Table 2 and 3.

Implementation of Control $u_1(t)$ ***only*** The impact of implementing control $u_1(t)$ alone is analyzed in Figure 5, highlighting the role of preventive measures in mitigating Mpox transmission. These measures, including the use of hand gloves when handling rodents, regular hand washing, and avoiding direct contact with open sores of infected individuals, aim to reduce the number of infections and lower the environmental concentration of MPXV. In figure 5(a), when the control $u_1(t)$ is implemented, the maximum number of Mpox infection in humans dropped from nearly 920 to 700 in week 22, and further decreases from around 450 to 35 within 100 weeks. Figure 5(b) indicates that when the control u_1 is implemented, the environmental concentration of MPXV decreases from 425 to around 370 in week 20, and further decreases from 310 to around 230 within 100 weeks. Figure 5(c) is the plot of the corresponding control profile u_1.

Implementation of Control $u_2(t)$ ***only*** Figure 6 illustrates the impact of the application of $u_2(t)$ only, which is the use of disinfectants (in washing of clothes and cleaning of surfaces) and proper sanitation practices to increase the decay rate of MPXV in the environment on the number of infected humans with Mpox and the concentration of Mpox virus in the environment. In figure 6(a), it is observed that when the control $u_2(t)$ is implemented, the maximum number of infected humans with Mpox dropped from around 920 to 775 in week 22, and further decreases from around 450 to 130 within 100 weeks. It is observed in figure 6(b) that when the control u_2 is implemented, the environmental concentration of MPXV decreases from 425 to around 100 in week 20, and further decreases from 310 to around 120 within 100 weeks . Figure 6(c) is the plot of the corresponding control profile u_2.

Implementation of Both Control $u_1(t)$ ***and Control*** $u_2(t)$ Figure 7 illustrates the impact of the implementation of both the controls $u_1(t)$ and $u_2(t)$ on the number of infected humans with Mpox and the concentration of Mpox virus in the environment. In figure 7(a), it is observed that when the controls $u_1(t)$ and $u_2(t)$ are implemented, the maximum number of infected humans with Mpox dropped from around 920 to 700 in week 22, and further decreases from around 450 to below 20 within 100 weeks. It is observed in figure 7(b) that when the controls $u_1(t)$ and $u_2(t)$ are

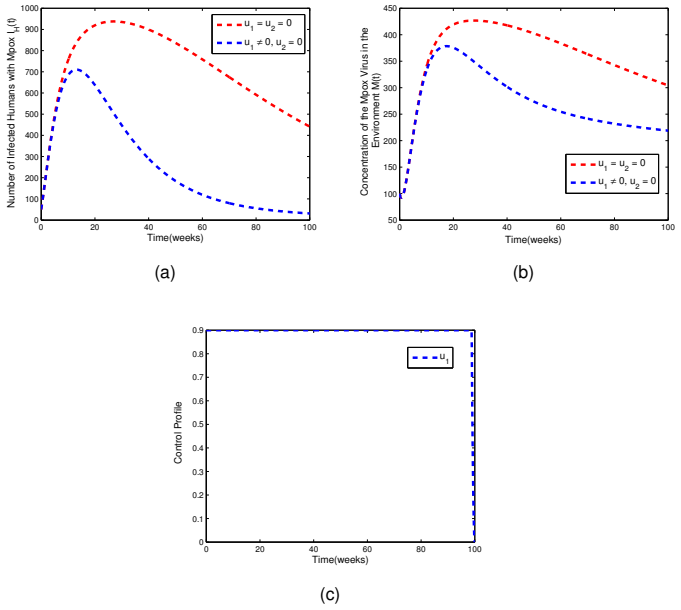

Figure 5 Simulation of (a) the implementation of u_1 on the number of infected humans with Mpox (b) the implementation of u_1 on the environmental concentration of the MPXV (c) the control profile u_1.

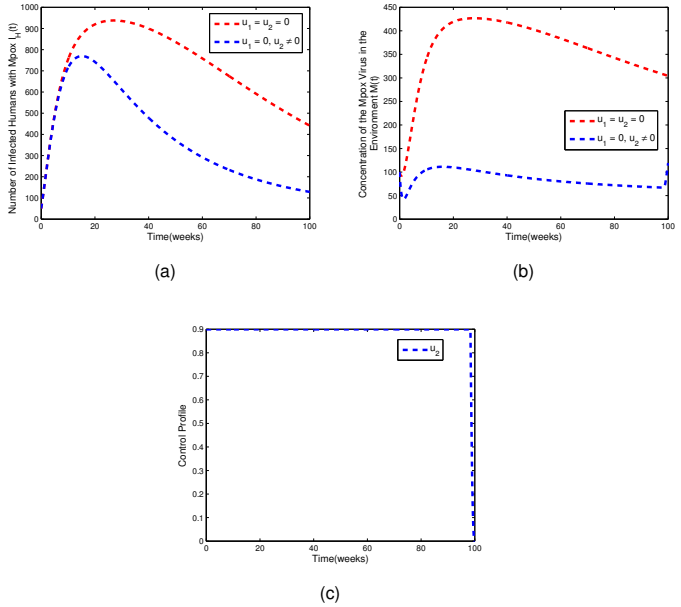

Figure 6 Simulation of (a)the impact of implementing control u_2 on the number of Mpox-infected humans (b) the effect of u_2 on the concentration of the Mpox virus in the environment(c) the control profile of u_2 over time.

implemented, the environmental concentration of MPXV decreases from 425 to around 100 in week 20, and further decreases from 310 to around 115 within 100 weeks . Figure 7(c) is the plot of the corresponding control profile u_1 and u_2.

The results indicate that the most effective strategy for controlling Mpox infection is the simultaneous implementation of precautionary measures adopted by susceptible individuals and

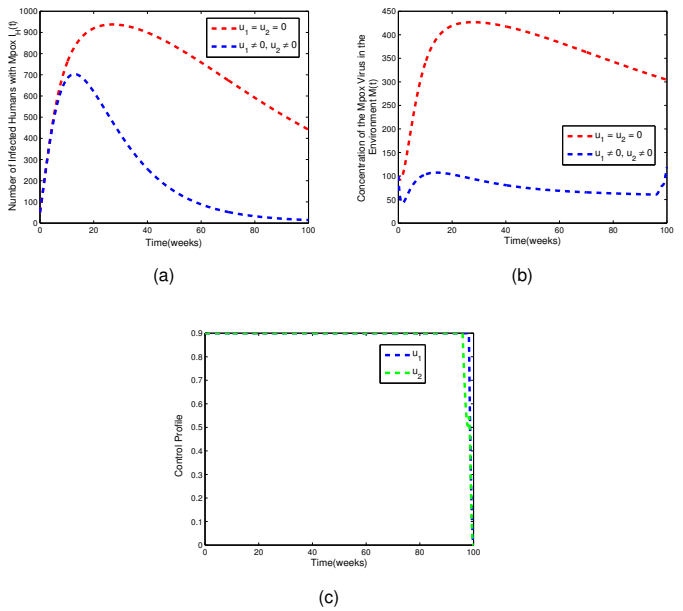

Figure 7 Simulation of (a) the implementation of both u_1 and u_2 on the number of infected humans with Mpox (b) the implementation of both u_1 and u_2 on the concentration of the Mpox virus in the environment(c) the control profile of both u_1 and u_2.

environmental disinfection interventions. The precautionary control, $u_1(t)$, includes regular hand washing, wearing gloves when handling rodents, and avoiding direct contact with open sores of infected individuals, all of which act to hinder the spread of Mpox. The environmental control, $u_2(t)$, involves the use of disinfectants for washing clothes and cleaning surfaces, as well as the adoption of proper sanitation practices to increase the decay rate of MPXV in the environment. The strong combined impact of these two control measures arises from their complementary effects on distinct yet tightly coupled transmission mechanisms within the model. The precautionary control $u_1(t)$ reduces direct transmission pathways by limiting human–rodent contact and decreasing exposure to contaminated hands and materials, thereby primarily lowering the rate at which new human infections occur. In contrast, the disinfection control $u_2(t)$ targets the environmental reservoir by accelerating the decay of MPXV on contaminated clothing and surfaces, which shortens the duration of environmental infectiousness. Mechanistically, these controls interact through a feedback loop linking infected hosts and environmental contamination: reduced contact decreases viral shedding into the environment, while enhanced disinfection accelerates viral removal. Together, these effects weaken both the introduction and persistence of environmental infection, disrupting a key mechanism responsible for disease persistence and backward bifurcation. Consequently, the combined implementation of both controls produces a synergistic effect that is substantially stronger than either intervention applied in isolation.

CONCLUSION

Understanding the dynamics of Mpox co-circulating within human and rodent populations is critical for designing effective prevention, surveillance, and control strategies. Comprehensive studies are needed that investigate the role of rodents in the transmission cycle, assess the risk of cross-species transmission, and evaluate long-term public health implications. Consequently, this study aims to expand the understanding and clarify the complexity underlying Mpox transmission dynamics in human and rodent populations by identifying and systematically analyzing the stability of Mpox boundary equilibria using a deterministic modeling framework. The identified boundary equilibria include the rodent-only equilibrium, the human-only equilibrium, and the coexistence equilibrium involving both human and rodent populations. The existence of rodent-only and human-only boundary equilibria mathematically demonstrates that Mpox can persist independently within each host population. From a biological perspective, this finding supports empirical evidence showing that rodents can maintain the monkeypox virus (MPXV) enzootically, while human populations can sustain outbreaks through close-contact transmission even in the absence of active zoonotic spillover. Using center manifold theory, it is shown that both the human-only and rodent-only boundary equilibria undergo backward bifurcation when the model-associated basic reproduction number is less than one. This backward bifurcation phenomenon complicates the eradication of Mpox in both human and animal populations, as disease persistence may occur even when the basic reproduction number is below the threshold value of one. Biologically, this reflects the ability of environmental viral persistence and reservoir hosts to maintain transmission despite reduced contact rates, highlighting the limitations of threshold-based control strategies.

To further assess the robustness of the model predictions and identify the key drivers of Mpox transmission, an uncertainty and sensitivity analysis based on Latin Hypercube Sampling and Partial Rank Correlation Coefficient methods was performed. The results reveal that the basic reproduction number is most sensitive to the human-to-human transmission rate, the rodent-to-rodent transmission rate, and the proportion of quarantined humans who progress to active infection. These parameters exhibit strong positive correlations with disease transmission, indicating that small increases in human contact rates, sustained transmission within rodent reservoirs, or ineffective quarantine measures can substantially exacerbate Mpox outbreaks. Conversely, the treatment rate of infected humans and the rodent death rate are strongly negatively correlated with the basic reproduction number, demonstrating that timely clinical management and reductions in the infectious rodent population play a critical role in suppressing transmission. These findings identify the parameters that contribute most to uncertainty in model outcomes and highlight priority targets for intervention and improved data collection. To emphasize the importance of community education, public awareness, and enlightenment campaigns in curbing the spread of Mpox, two time-dependent control measures were incorporated into the model. The first includes preventive behavioral interventions aimed at reducing susceptibility to infection, such as wearing gloves when handling rodents, regular handwashing, and avoiding direct contact with the open lesions of infected individuals. The second involves environmental disinfection, including washing clothes, cleaning contaminated surfaces, and implementing proper sanitation practices to increase the decay rate of the virus in the environment.

Numerical simulations indicate that while each control strategy independently reduces Mpox transmission, the combined implementation of both interventions is significantly more effective in lowering disease prevalence. Optimal control simulations further reveal that precautionary behavioral measures alone can reduce infection incidence but may be insufficient for disease elimination,

whereas environmental disinfection is most effective when combined with behavioral interventions. Biologically, this suggests that effective Mpox control requires the simultaneous reduction of human exposure and environmental viral persistence. Overall, the model demonstrates that Mpox persistence is driven by interacting biological mechanisms, including sustained transmission within rodent reservoirs, environmental survival of the virus, and human behavioral factors. These mechanisms are captured mathematically through coupled nonlinear dynamics, backward bifurcation behavior, and sensitivity patterns, providing a comprehensive understanding of the complexity underlying Mpox transmission and control. The combined analytical, numerical, and uncertainty-based findings reinforce the need for integrated intervention strategies targeting both human and animal populations, as well as environmental pathways, to achieve effective and sustainable Mpox control.

APPENDIX

$$
\begin{aligned}
\mathscr{C}_1 &= -\Lambda_1\left(\frac{(1-u_1(t))(\beta_H I_H+\beta_{RH} I_R)S_H}{N_H^2}-\right.\\
&\quad \left.(1-u_1(t))\left(\frac{\beta_H I_H+\beta_{RH} I_R}{N_H}+\frac{\beta_{eH} M}{K+M}\right)-\omega_H\right)+\\
&\quad \Lambda_2\left(\frac{(1-u_1(t))(\beta_H I_H+\beta_{RH} I_R)S_H}{N_H^2}-\right.\\
&\quad \left.(1-u_1(t))\left(\frac{\beta_H I_H+\beta_{RH} I_R}{N_H}+\frac{\beta_{eH} M}{K+M}\right)\right)+\\
&\quad \frac{\Lambda_4(1-u_1(t))\varphi(\beta_H I_H+\beta_{RH} I_R)R_H}{N_H^2}-\\
&\quad \frac{\Lambda_6(1-u_1(t))\varphi(\beta_H I_H+\beta_{RH} I_R)R_H}{N_H^2},\\
\mathscr{C}_2 &= -\frac{\Lambda_1(1-u_1(t))(\beta_H I_H+\beta_{RH} I_R)S_H}{N_H^2}+\\
&\quad \Lambda_2\left(\frac{(1-u_1(t))(\beta_H I_H+\beta_{RH} I_R)S_H}{N_H^2}+\gamma+\psi+\omega_H\right)-\\
&\quad \Lambda_3\gamma+\Lambda_4\left(\frac{(1-u_1(t))\varphi(\beta_H I_H+\beta_{RH} I_R)R_H}{N_H^2}-\psi\right)-\\
&\quad \frac{\Lambda_6(1-u_1(t))\varphi(\beta_H I_H+\beta_{RH} I_R)R_H}{N_H^2},\\
\mathscr{C}_3 &= -\Lambda_1\left(\frac{(1-u_1(t))(\beta_H I_H+\beta_{RH} I_R)S_H}{N_H^2}+(1-\alpha)\sigma\right)+\\
&\quad \frac{\Lambda_2(1-u_1(t))(\beta_H I_H+\beta_{RH} I_R)S_H}{N_H^2}+\\
&\quad \Lambda_3(\sigma+\omega_H)+\Lambda_4\left(\frac{(1-u_1(t))\varphi(\beta_H I_H+\beta_{RH} I_R)R_H}{N_H^2}-\alpha\sigma\right)\\
&\quad -\frac{\Lambda_6(1-u_1(t))\varphi(\beta_H I_H+\beta_{RH} I_R)R_H}{N_H^2},\\
\mathscr{C}_4 &= -\mathscr{B}_1+\Lambda_1\left(\xi\pi_H+\right.\\
&\quad \left.(1-u_1(t))\left(\frac{\beta_H}{N_H}-\frac{\beta_H I_H+\beta_{RH} I_R}{N_H^2}\right)S_H\right)\\
&\quad -\Lambda_2(1-u_1(t))\left(\frac{\beta_H}{N_H}-\frac{\beta_H I_H+\beta_{RH} I_R}{N_H^2}\right)S_H+\\
&\quad \Lambda_6(1-u_1(t))\varphi\left(\frac{\beta_H}{N_H}-\frac{\beta_H I_H+\beta_{RH} I_R}{N_H^2}\right)R_H-\\
&\quad \Lambda_4\left(\xi\pi_H+(1-u_1(t))\varphi\left(\frac{\beta_H}{N_H}-\frac{\beta_H I_H+\beta_{RH} I_R}{N_H^2}\right)R_H-\right.\\
&\quad \left.\tau-\delta_H-\omega_H\right)-\Lambda_5\tau-\Lambda_{10}r_2,\\
\mathscr{C}_5 &= -\frac{\Lambda_1(1-u_1(t))(\beta_H I_H+\beta_{RH} I_R)S_H}{N_H^2}+\\
&\quad \frac{\Lambda_2(1-u_1(t))(\beta_H I_H+\beta_{RH} I_R)S_H}{N_H^2}+\\
&\quad \Lambda_5(\theta+\phi\delta_H+\omega_H)\\
&\quad +\frac{\Lambda_4(1-u_1(t))\varphi(\beta_H I_H+\beta_{RH} I_R)R_H}{N_H^2}-\\
&\quad \Lambda_6\left(\frac{(1-u_1(t))\varphi(\beta_H I_H+\beta_{RH} I_R)R_H}{N_H^2}+\theta\right),\\
\mathscr{C}_6 &= -\frac{\Lambda_1(1-u_1(t))(\beta_H I_H+\beta_{RH} I_R)S_H}{N_H^2}+\\
&\quad \frac{\Lambda_2(1-u_1(t))(\beta_H I_H+\beta_{RH} I_R)S_H}{N_H^2}+\\
&\quad \Lambda_4\left(\frac{(1-u_1(t))\varphi(\beta_H I_H+\beta_{RH} I_R)R_H}{N_H^2}-\right.\\
&\quad \left.(1-u_1(t))\varphi\left(\frac{\beta_H I_H+\beta_{RH} I_R}{N_H}+\frac{\beta_{eH} M}{K+M}\right)\right)-\\
&\quad \Lambda_6\left(\frac{(1-u_1(t))\varphi(\beta_H I_H+\beta_{RH} I_R)R_H}{N_H^2}-\right.\\
&\quad \left.(1-u_1(t))\varphi\left(\frac{\beta_H I_H+\beta_{RH} I_R}{N_H}+\frac{\beta_{eH} M}{K+M}\right)-\omega_H\right),\\
\mathscr{C}_7 &= -\Lambda_7\left(\frac{\beta_R I_R S_R}{N_R^2}-\frac{\beta_R I_R}{N_R}-\frac{\beta_{eR} M}{K+M}-\omega_R\right)+\\
&\quad \Lambda_8\left(\frac{\beta_R I_R S_R}{N_R^2}-\frac{\beta_R I_R}{N_R}-\frac{\beta_{eR} M}{K+M}\right),\\
\mathscr{C}_8 &= -\frac{\Lambda_7\beta_R I_R S_R}{N_R^2}+\Lambda_8\left(\frac{\beta_R I_R S_R}{N_R^2}+\eta+\omega_R\right)-\Lambda_9\eta,\\
\mathscr{C}_9 &= \frac{\Lambda_1(1-u_1(t))\beta_{RH} S_H}{N_H}-\frac{\Lambda_2(1-u_1(t))\beta_{RH} S_H}{N_H}-\\
&\quad \frac{\Lambda_4(1-u_1(t))\varphi\beta_{RH} R_H}{N_H}+\frac{\Lambda_6(1-u_1(t))\varphi\beta_{RH} R_H}{N_H}\\
&\quad +\Lambda_7\left(\frac{\beta_R}{N_R}-\frac{\beta_R I_R}{N_R^2}\right)S_R-\Lambda_8\left(\frac{\beta_R}{N_R}-\frac{\beta_R I_R}{N_R^2}\right)S_R+\\
&\quad \Lambda_9\omega_R-\Lambda_{10}r_1,\\
\mathscr{C}_{10} &= \Lambda_1(1-u_1(t))\left(\frac{\beta_{eH}}{K+M}-\frac{\beta_{eH} M}{(K+M)^2}\right)S_H-\\
&\quad \Lambda_2(1-u_1(t))\left(\frac{\beta_{eH}}{K+M}-\frac{\beta_{eH} M}{(K+M)^2}\right)S_H-\\
&\quad \Lambda_4(1-u_1(t))\varphi\left(\frac{\beta_{eH}}{K+M}-\frac{\beta_{eH} M}{(K+M)^2}\right)R_H+\\
&\quad \Lambda_6(1-u_1(t))\varphi\left(\frac{\beta_{eH}}{K+M}-\frac{\beta_{eH} M}{(K+M)^2}\right)R_H+\\
&\quad \Lambda_7\left(\frac{\beta_{eR}}{K+M}-\frac{\beta_{eR} M}{(K+M)^2}\right)S_R-\\
&\quad \Lambda_8\left(\frac{\beta_{eR}}{K+M}-\frac{\beta_{eR} M}{(K+M)^2}\right)S_R+\Lambda_{10}(\omega_e+u_2(t)).
\end{aligned}
$$

Availability of Data and material

Not applicable.

Conflicts of interest

The authors declare that there is no conflict of interest regarding the publication of this paper.

Ethical standard

The authors have no financial or non-financial interests to disclose.

LITERATURE CITED

Adepoju, O. and H. Ibrahim, 2024 An optimal control model for monkeypox transmission dynamics with vaccination and immunity loss following recovery. Healthcare Analytics **6**: 100355.

Ahmad, Y. U., J. Andrawus, A. Ado, Y. A. Maigoro, A. Yusuf, *et al.*, 2024 Mathematical modeling and analysis of human-to-human monkeypox virus transmission with post-exposure vaccination. Modeling Earth Systems and Environment **10**: 2711–2731.

Al-Shomrani, M. M., S. S. Musa, and A. Yusuf, 2023 Unfolding the transmission dynamics of monkeypox virus: an epidemiological modelling analysis. Mathematics **11**: 1121.

Alharbi, R., R. Jan, S. Alyobi, Y. Altayeb, and Z. Khan, 2022 Mathematical modeling and stability analysis of the dynamics of monkeypox via fractional-calculus. Fractals **30**: 2240266.

Aly, E. S., M. Singh, M. A. Aiyashi, and M. D. Albalwi, 2024 Modeling monkeypox virus transmission: Stability analysis and comparison of analytical techniques. Open Physics **22**: 20240056.

Araf, Y., J. F. Nipa, S. Naher, S. T. Maliha, H. Rahman, *et al.*, 2024 Insights into the transmission, host range, genomics, vaccination, and current epidemiology of the monkeypox virus. Veterinary Medicine International **2024**: 8839830.

Banuet-Martinez, M., Y. Yang, B. Jafari, A. Kaur, Z. A. Butt, *et al.*, 2023 Monkeypox: a review of epidemiological modelling studies and how modelling has led to mechanistic insight. Epidemiology & Infection **151**: e121.

Boubaker, O., 2024 Chaos in physiological control systems: Health or disease? Chaos Theory and Applications **6**: 1–12.

Branda, F., C. Romano, M. Ciccozzi, M. Giovanetti, F. Scarpa, *et al.*, 2024 Mpox: an overview of pathogenesis, diagnosis, and public health implications. Journal of Clinical Medicine **13**: 2234.

Castillo-Chavez, C. and B. Song, 2004 Dynamical models of tuberculosis and their applications. Mathematical biosciences and engineering **1**: 361.

El Mansouri, A., I. Smouni, B. Khajji, A. Labzai, and M. Belam, 2023 Mathematical modeling and optimal control strategy for the monkeypox epidemic. Math Model Comput **10**: 944–955.

Elsonbaty, A., W. Adel, A. Aldurayhim, and A. El-Mesady, 2024 Mathematical modeling and analysis of a novel monkeypox virus spread integrating imperfect vaccination and nonlinear incidence rates. Ain Shams Engineering Journal **15**: 102451.

Fleming, W. H. and R. W. Rishel, 2012 *Deterministic and stochastic optimal control*. Springer Science & Business Media.

Gumel, A. B., 2012 Causes of backward bifurcations in some epidemiological models. Journal of Mathematical Analysis and Applications **395**: 355–365.

Gumel, A. B., J. M.-S. Lubuma, O. Sharomi, and Y. A. Terefe, 2018 Mathematics of a sex-structured model for syphilis transmission dynamics. Mathematical Methods in the Applied Sciences **41**: 8488–8513.

Islam, M. A., J. Mumin, M. M. Haque, M. A. Haque, A. Khan, *et al.*, 2023 Monkeypox virus (mpxv): A brief account of global spread, epidemiology, virology, clinical features, pathogenesis, and therapeutic interventions. Infectious medicine **2**: 262–272.

Jose, S. A., R. Raja, J. Alzabut, G. Rajchakit, J. Cao, *et al.*, 2022 Mathematical modeling on transmission and optimal control strategies of corruption dynamics. Nonlinear Dynamics **109**: 3169–3187.

Jose, S. A., R. Raja, J. Dianavinnarasi, D. Baleanu, and A. Jirawattanapanit, 2023a Mathematical modeling of chickenpox in phuket: Efficacy of precautionary measures and bifurcation analysis. Biomedical Signal Processing and Control **84**: 104714.

Jose, S. A., R. Raja, B. Omede, R. P. Agarwal, J. Alzabut, *et al.*, 2023b Mathematical modeling on co-infection: transmission dynamics of zika virus and dengue fever. Nonlinear Dynamics **111**: 4879–4914.

Kaler, J., A. Hussain, G. Flores, S. Kheiri, and D. Desrosiers, 2022 Monkeypox: a comprehensive review of transmission, pathogenesis, and manifestation. Cureus **14**.

Kang, T.-L., H.-F. Huo, and H. Xiang, 2024 Dynamics and optimal control of tuberculosis model with the combined effects of vaccination, treatment and contaminated environments. Mathematical Biosciences and Engineering **21**: 5308–5334.

Kumar, N., A. Acharya, H. E. Gendelman, and S. N. Byrareddy, 2022 The 2022 outbreak and the pathobiology of the monkeypox virus. Journal of autoimmunity **131**: 102855.

Larkin, M., 2003 Monkeypox spreads as us public-health system plays catch-up. The Lancet Infectious Diseases **3**: 461.

Lenhart, S. and J. T. Workman, 2007 *Optimal control applied to biological models*. Chapman and Hall/CRC.

Lum, F.-M., A. Torres-Ruesta, M. Z. Tay, R. T. Lin, D. C. Lye, *et al.*, 2022 Monkeypox: disease epidemiology, host immunity and clinical interventions. Nature Reviews Immunology **22**: 597–613.

Mitjà, O., D. Ogoina, B. K. Titanji, C. Galvan, J.-J. Muyembe, *et al.*, 2023 Monkeypox. The Lancet **401**: 60–74.

Oguntolu, F. A., O. J. Peter, B. I. Omede, G. B. Balogun, and T. A. Ayoola, 2025 Mathematical model on the transmission dynamics of leptospirosis in human and animal population with optimal control strategies using real statistical data. Quality & Quantity **59**: 1405–1444.

Okongo, W., J. A. Okelo, D. K. Gathungu, S. E. Moore, and S. A. Nnaemeka, 2024 Transmission dynamics of monkeypox virus with age-structured human population: A mathematical modeling approach. Journal of Applied Mathematics **2024**: 9173910.

Omame, A., M. Abbas, and C. P. Onyenegecha, 2022 Backward bifurcation and optimal control in a co-infection model for sars-cov-2 and zikv. Results in Physics **37**: 105481.

Omame, A., N. Sene, I. Nometa, C. I. Nwakanma, E. U. Nwafor, *et al.*, 2021 Analysis of covid-19 and comorbidity co-infection model with optimal control. Optimal Control Applications and Methods **42**: 1568–1590.

Omede, B., U. Odionyenma, A. Ibrahim, and B. Bolaji, 2023a Third wave of covid-19: mathematical model with optimal control strategy for reducing the disease burden in nigeria. International Journal of Dynamics and control **11**: 411–427.

Omede, B. I., B. Bolaji, O. J. Peter, A. A. Ibrahim, and F. A. Oguntolu, 2024a Mathematical analysis on the vertical and horizontal transmission dynamics of hiv and zika virus co-infection. Franklin Open **6**: 100064.

Omede, B. I., S. Jose, and O. Boubaker, 2026 Modeling mpox transmission dynamics. In *AI and Data Science in Medical Research.*, Academic Press (Elsevier).

Omede, B. I., S. A. Jose, J. Anuwat, and T. Park, 2024b Mathematical analysis on the transmission dynamics of delta and omicron variants of covid-19 in the united states. Modeling Earth Systems and Environment pp. 1–38.

Omede, B. I., O. J. Peter, W. Atokolo, B. Bolaji, and T. A. Ayoola, 2023b A mathematical analysis of the two-strain tuberculosis model dynamics with exogenous re-infection. Healthcare Analytics **4**: 100266.

Peter, O. J., C. E. Madubueze, M. M. Ojo, F. A. Oguntolu, and T. A. Ayoola, 2023 Modeling and optimal control of monkeypox with cost-effective strategies. Modeling Earth Systems and Environment **9**: 1989–2007.

Peter, O. J., F. A. Oguntolu, M. M. Ojo, A. Olayinka Oyeniyi, R. Jan, *et al.*, 2022 Fractional order mathematical model of monkeypox transmission dynamics. Physica Scripta **97**: 084005.

Pontryagin, L. S., 2018 *Mathematical theory of optimal processes*. Routledge.

Qureshi, M., S. Khan, R. A. Bantan, M. Daniyal, M. Elgarhy, *et al.*, 2022 Modeling and forecasting monkeypox cases using stochastic models. Journal of Clinical Medicine **11**: 6555.

Reed, K. D., J. W. Melski, M. B. Graham, R. L. Regnery, M. J. Sotir, *et al.*, 2004 The detection of monkeypox in humans in the western hemisphere. New England Journal of Medicine **350**: 342–350.

Schwartz, D. A., P. Mbala-Kingebeni, K. Patterson, J. W. Hug-

gins, and P. R. Pittman, 2023 Congenital mpox syndrome (clade i) in stillborn fetus after placental infection and intrauterine transmission, democratic republic of the congo, 2008. Emerging Infectious Diseases **29**: 2198.
Statista, 2025a Birth rate in nigeria from 2012 to 2022. Accessed: 2025-09-20.
Statista, 2025b Death rate in nigeria from 2012 to 2022. Accessed: 2025-09-20.
Stephenson, J., 2003 Monkeypox outbreak a reminder of emerging infections vulnerabilities. Jama **290**: 23–24.
Subissi, L., P. Stefanelli, and G. Rezza, 2024 Human mpox: global trends, molecular epidemiology and options for vaccination. Pathogens and global health **118**: 25–32.
Sun, Y., W. Nie, D. Tian, and Q. Ye, 2024 Human monkeypox virus: Epidemiologic review and research progress in diagnosis and treatment. Journal of Clinical Virology **171**: 105662.
Sweilam, N., Z. Mohammed, and W. A. Kareem, 2024 Numerical approaches for solving complex order monkeypox mathematical model. Alexandria Engineering Journal **90**: 170–182.
Thornhill, J. P., S. Barkati, S. Walmsley, J. Rockstroh, A. Antinori, *et al.*, 2022 Monkeypox virus infection in humans across 16 countries—april–june 2022. New England Journal of Medicine **387**: 679–691.
Van den Driessche, P. and J. Watmough, 2002 Reproduction numbers and sub-threshold endemic equilibria for compartmental models of disease transmission. Mathematical biosciences **180**: 29–48.
Wiraya, A., Y. A. Adi, L. Fitriana, T. Triyanto, Y. A. Kusumadewi, *et al.*, 2024 Birth of catastrophe and strange attractors through generalized hopf bifurcations in covid-19 transmission mathematical model. Chaos Theory and Applications **6**: 159–169.
World Health Organization *et al.*, 2022 Who recommends new name for monkeypox disease.
Yılmaz, E. and E. Aydıner, 2024 Chaotic and quasi-periodic regimes in the covid-19 mortality data. Chaos Theory and Applications **6**: 41–50.

How to cite this article: Omede, B. I., Jose, S. A., Jirawattanapanit, A., and Boubaker, O. Stability and Bifurcation Analysis of Mpox Transmission Model. *Chaos Theory and Applications*, 8(1), 36-55, 2026.